

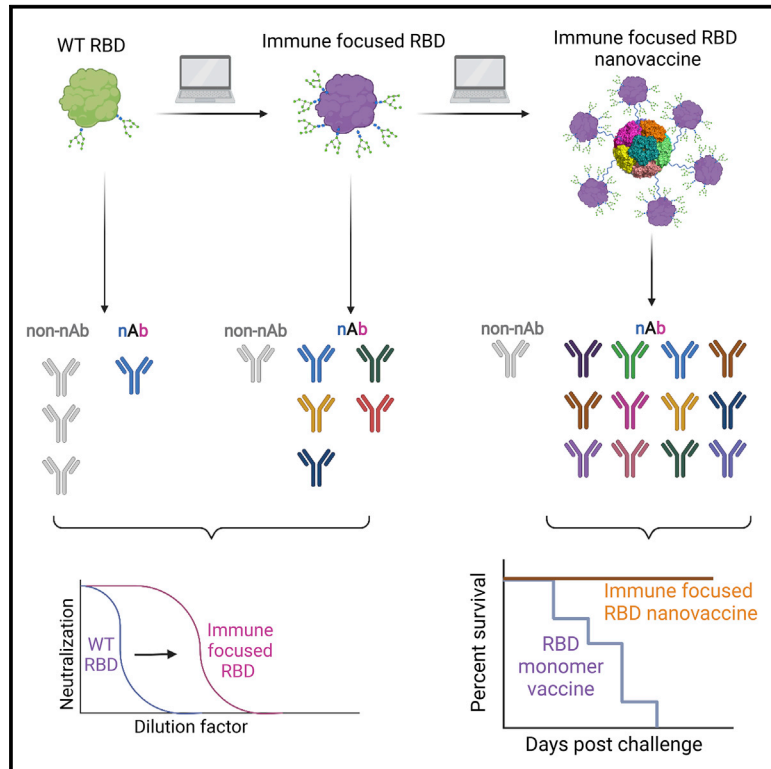


Since January 2020 Elsevier has created a COVID-19 resource centre with free information in English and Mandarin on the novel coronavirus COVID-19. The COVID-19 resource centre is hosted on Elsevier Connect, the company's public news and information website.

Elsevier hereby grants permission to make all its COVID-19-related research that is available on the COVID-19 resource centre - including this research content - immediately available in PubMed Central and other publicly funded repositories, such as the WHO COVID database with rights for unrestricted research re-use and analyses in any form or by any means with acknowledgement of the original source. These permissions are granted for free by Elsevier for as long as the COVID-19 resource centre remains active.

## Nucleic acid delivery of immune-focused SARS-CoV-2 nanoparticles drives rapid and potent immunogenicity capable of single-dose protection

### Graphical abstract



### Authors

Kylie M. Konrath, Kevin Liaw, Yuanhan Wu, ..., Jesper Pallesen, David B. Weiner, Daniel W. Kulp

### Correspondence

dwkulp@wistar.org

### In brief

Glycan engineering of immunogens is a key vaccine design strategy to focus antibodies to select epitopes. Konrath et al. create an automated pipeline to screen SARS-CoV-2 RBD for PNGS. PNGS-modified RBDs elicit enhanced ACE2-directed responses and higher neutralization. Multivalent display of glycan-engineered RBDs delivered via nucleic acid provides single-dose protection from challenge.

### Highlights

- Development of an automated pipeline “CWG” to screen the SARS-CoV-2 RBD for PNGS
- RBD can be glycan modified for custom immune responses with improved neutralization
- Glycan-modified RBD nanoparticles delivered via nucleic acid elicit strong responses against VOCs
- RBD nanoparticles provide protection from lethal challenge with a single low dose



## Article

# Nucleic acid delivery of immune-focused SARS-CoV-2 nanoparticles drives rapid and potent immunogenicity capable of single-dose protection

Kylie M. Konrath,<sup>1,2,8</sup> Kevin Liaw,<sup>1,8</sup> Yuanhan Wu,<sup>1,8</sup> Xizhou Zhu,<sup>1,8</sup> Susanne N. Walker,<sup>1,8</sup> Ziyang Xu,<sup>1,2,8</sup> Katherine Schultheis,<sup>3,8</sup> Neethu Chokkalingam,<sup>1,8</sup> Himanshi Chawla,<sup>4</sup> Jianqiu Du,<sup>5</sup> Nicholas J. Tursi,<sup>1</sup> Alan Moore,<sup>5</sup> Jared Adolf-Bryfogle,<sup>6</sup> Mansi Purwar,<sup>1</sup> Emma L. Reuschel,<sup>1</sup> Drew Frase,<sup>1</sup> Matthew Sullivan,<sup>2</sup> Benjamin Fry,<sup>1</sup> Igor Maricic,<sup>3</sup> Viviane M. Andrade,<sup>3</sup> Christel Iffland,<sup>7</sup> Max Crispin,<sup>4</sup> Kate E. Broderick,<sup>3</sup> Laurent M.P.F. Humeau,<sup>3</sup> Ami Patel,<sup>1</sup> Trevor R.F. Smith,<sup>3</sup> Jesper Pallesen,<sup>6</sup> David B. Weiner,<sup>1</sup> and Daniel W. Kulp<sup>1,2,9,\*</sup>

<sup>1</sup>Vaccine and Immunotherapy Center, The Wistar Institute, Philadelphia, PA 19104, USA

<sup>2</sup>Perelman School of Medicine, University of Pennsylvania, Philadelphia, PA 19104, USA

<sup>3</sup>Inovio Pharmaceuticals, Plymouth Meeting, PA 19462, USA

<sup>4</sup>School of Biological Sciences, University of Southampton, Southampton SO17 1BJ, UK

<sup>5</sup>Molecular and Cellular Biochemistry, Indiana University, Bloomington, IN 47405, USA

<sup>6</sup>Institute for Protein Innovation, Boston, MA 02115, USA

<sup>7</sup>Ligand Pharmaceuticals Inc., San Diego, CA 92121, USA

<sup>8</sup>These authors contributed equally

<sup>9</sup>Lead contact

\*Correspondence: [dwkulp@wistar.org](mailto:dwkulp@wistar.org)

<https://doi.org/10.1016/j.celrep.2022.110318>

## SUMMARY

Severe acute respiratory syndrome coronavirus 2 (SARS-CoV-2) vaccines may target epitopes that reduce durability or increase the potential for escape from vaccine-induced immunity. Using synthetic vaccinology, we have developed rationally immune-focused SARS-CoV-2 Spike-based vaccines. Glycans can be employed to alter antibody responses to infection and vaccines. Utilizing computational modeling and *in vitro* screening, we have incorporated glycans into the receptor-binding domain (RBD) and assessed antigenic profiles. We demonstrate that glycan-coated RBD immunogens elicit stronger neutralizing antibodies and have engineered seven multivalent configurations. Advanced DNA delivery of engineered nanoparticle vaccines rapidly elicits potent neutralizing antibodies in guinea pigs, hamsters, and multiple mouse models, including human ACE2 and human antibody repertoire transgenics. RBD nanoparticles induce high levels of cross-neutralizing antibodies against variants of concern with durable titers beyond 6 months. Single, low-dose immunization protects against a lethal SARS-CoV-2 challenge. Single-dose coronavirus vaccines via DNA-launched nanoparticles provide a platform for rapid clinical translation of potent and durable coronavirus vaccines.

## INTRODUCTION

Severe acute respiratory syndrome coronavirus 2 (SARS-CoV-2) virus is responsible for coronavirus disease 2019 (COVID-19) in over 350 million people and 5.5 million deaths as of January 24, 2022 (Dong et al., 2020; Elbe and Buckland-Merrett, 2017). The Spike (S) glycoprotein studs the surface of coronaviruses virions, and its receptor-binding domain (RBD) binds host cell receptors to mediate viral entry and infection (Letko et al., 2020; Zhou et al., 2020b). More than 90% of COVID-19 patients produce neutralizing antibodies (nAbs) (Wajnberg et al., 2020), and RBD-directed antibodies often comprise 90% of the total neutralizing response (Piccoli et al., 2020). RBD-directed antibodies can correlate with neutralizing activity (Byrnes et al., 2020; Suthar et al., 2020; Wang et al., 2015), and ~2,500 anti-

bodies targeting the SARS-CoV-2 spike have been described to date (Yuan et al., 2020a; Raybould et al., 2020). This highlights the importance of eliciting nAbs targeting the RBD by vaccination.

Rational SARS-CoV-2 vaccine design should be informed by S protein conformation dynamics, the sites of vulnerability, and mutations that cause potential vaccine escape. The S trimer has >3,000 residues, creating a vast array of epitopes, and is targeted by both nAbs and non-neutralizing antibodies (non-nAbs) (Brouwer et al., 2020; Ju et al., 2020; Liu et al., 2020; Rogers et al., 2020). Measures of RBD binding do not always correlate with neutralization due to presence of non-nAbs, which have the potential to cause antibody-dependent enhancement (Wu et al., 2020; Yazici et al., 2020; Lee et al., 2020). In the context of HIV, influenza, and Middle East respiratory syndrome-related



coronavirus (MERS-CoV), significant effort over the last few decades has focused on creating immunogens that minimize non-neutralizing epitopes (De Taeye et al., 2018; Kulp et al., 2017; Sanders et al., 2013; Ren and Zhou, 2016; Impagliazzo et al., 2015; Krammer and Palese, 2013; Yassine et al., 2015; Du et al., 2016). Since the initial outbreak of SARS-CoV-2, significant headway has been made in identifying neutralizing epitopes, especially with regards to the RBD; however, study of immunodominant, non-neutralizing epitopes has lagged (Barnes et al., 2020; Liu et al., 2020; Wu et al., 2020a). Vaccine immunogens should be developed with these key findings in mind.

Glycosylation is an important post-translational modification in viral pathogenesis serving versatile roles, including host cell trafficking and viral protein folding (Watanabe et al., 2019). Mutations introducing potential N-linked glycosylation sites (PNGSs) (Hariharan and Kane, 2020) in other viruses, such as HIV and influenza, have contributed to immune escape (Ly and Stamatos, 2000; Medina et al., 2013; Wanzeck et al., 2011; Wei et al., 2003). Structure-based vaccine design efforts have been employed to add exogenous PNGSs to block non-neutralizing sites and focus the immune response to neutralizing sites (Bajic et al., 2019; Kulp et al., 2017; Du et al., 2016; Ingale et al., 2014). These approaches have not yet been widely applied to SARS-CoV-2 vaccine development (Shinnakasu et al., 2021). Here, we develop an advanced structural algorithm for optimizing PNGSs into the SARS-CoV-2 RBD to focus the immune response and enhance neutralizing responses targeting the receptor binding site epitope (RBS).

Vaccine potency and durability are important for an effective immunological response. Self-assembling, multivalent nanoparticle immunogens (or nanovaccines) enhance the B cell activation and concomitant humoral responses, kinetics of trafficking to the draining lymph nodes, and uptake by dendritic cells and macrophages (Xu et al., 2020b, 2020c; Manolova et al., 2008; Kelly et al., 2019). SARS-CoV-2 nanovaccines developed as recombinant proteins can be difficult to clinically translate due to arduous purification and manufacturing processes and further do not tend to activate CD8<sup>+</sup> T cells (Xu et al., 2020c). In contrast, vaccine antigens encoded as a DNA plasmid can be delivered directly *in vivo*. We recently demonstrated the speed of DNA vaccine translation by developing a DNA-encoded full-length spike immunogen for clinical evaluation in 10 weeks (Smith et al., 2020). DNA is easily mass produced, temperature stable, not associated with anti-vector immunity, and can be rapidly reformulated for circulating variants, making it a key pandemic vaccine technology. We recently developed a DNA-launched nanoparticle platform (DLNP) for *in vivo* assembly of nanoparticles that drive rapid and strong B cell immunity and produce strong CD8<sup>+</sup> T cells (Xu et al., 2020c). Here, we present a SARS-CoV-2 DLNP that has enhanced immunity in multiple animal models, drives significantly durable immunity, and is capable of conferring single-shot protection against lethal challenge. The single-shot, low-dose regimen reduces the overall amount of necessary product, medical personnel, and time in the clinic, rendering the product more scalable to a global scope, including resource-limited settings. The high potency and rapid developability of the DLNP platform can also enable quick generation of

booster vaccines for newly emergent variants. To this end, we developed a SARS-CoV-2 DLNP encoding P.1 (Gamma) mutations and demonstrate it is highly immunogenic.

## RESULTS

### Mapping antigenic effects of N-linked glycans on the RBD

To assess the feasibility of adding N-linked glycans to alter antibody responses to RBD (Figure 1A), we built an advanced structural algorithm called cloaking with glycans (CWG) for modeling every possible glycan on the RBD (Figure 1B). The PNGS positions were filtered if the asparagine had low solvent accessibility or high clash score (Figure 1C). Next, we surveyed energetics of naturally occurring glycans (Figures S1A and S1B) and employed glycan energy filters for our designed glycan positions, as well as filters for protein-folding energies and structural considerations (see STAR Methods). This process led to the identification of 43 out of 196 positions for experimental characterization (Figures 1C and 1D).

To assess the impact on RBDs harboring single-glycan mutants (Figure 2A) *in vitro*, we produced each variant and measured biophysical and antigenic profiles. We synthesized and screened the glycan variants for expression and binding to ACE2 in a high-throughput, small-scale transfection format and downselected to 22 variants for further evaluation (Figure 2B). To characterize the antigenic properties of the glycan variants, we utilized 14 RBD-directed nAbs, 2 Abs with inconsistent neutralization (Huo et al., 2020; Yuan et al., 2020b; Zhou et al., 2020a; Seydoux et al., 2020), and 6 non-nAbs (Hansen et al., 2020; Wu et al., 2020b; Seydoux et al., 2020; Shi et al., 2020; Rogers et al., 2020; Pinto et al., 2020; Zhou et al., 2020a; Robbiani et al., 2020; Ju et al., 2020; Brouwer et al., 2020; Tian et al., 2020; Yuan et al., 2020a). Most nAbs target epitopes in the RBS (RBD-A, RBD-B, and RBD-C; Yuan et al., 2020a), and some target outside the RBS (Barnes et al., 2020; RBD-D, RBD-E, and RBD-F; Figure 2C). In general, we sought to identify glycans that do not interfere with nAb binding and block non-nAbs. The reactivity of our set of antibodies to each glycan mutant was determined by surface plasmon resonance (SPR) and ELISA (Figures 2D and 2E; Table S1). We observed reduced binding of neutralizing RBD-A, RBD-B, RBD-C, or RBD-D antibodies in the presence of glycans at residues 441 (RBD-D); 448, 450, and 481 (RBD-B and -C); and 458 (RBD-A). Glycans at these five positions do not significantly impact ACE2 binding, suggesting SARS-CoV-2 variant viruses harboring spike proteins with these glycans could evade immune pressure against those epitopes. In addition, glycans at positions 337, 344, 354, 357, 360, 369, 383, 448, 450, 516, and 521 show dramatically reduced binding to non-nAb(s). We did not observe effects on binding to our antibody panel for glycans at 518, 519, and 520. We noticed similar antigenic patterns in glycan positions that reduce binding to some of the non-nAbs as well as nAbs in RBS-E and RBS-F, suggesting there is overlap in these nAb and non-nAb epitopes. In sum, our experimental screening exhaustively evaluated the effect of N-linked glycans on the expression and antigenic profile of the RBD.

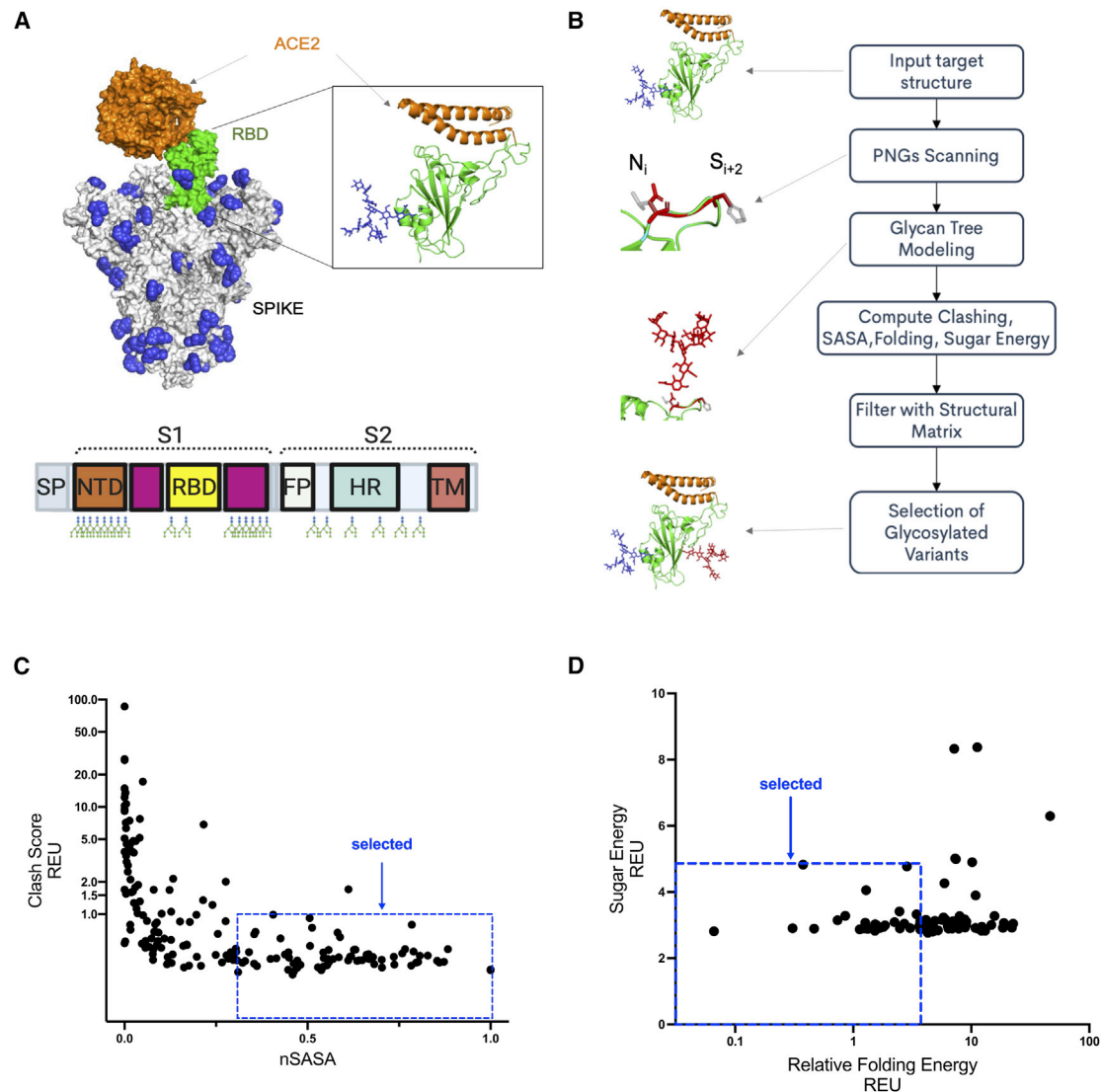


**Figure 1. CWG algorithm to identify sites amenable to glycosylation**

(A) SARS-CoV-2 spike trimer (gray) decorated with native glycans (blue) with one RBD in the up state (green) binding to ACE2 (orange) and detailed cartoon representation of RBD with native glycan bound to ACE2. Schematic of wild-type glycan distribution across the entire spike is shown.

(B) CWG pipeline for assessing PNGS on the RBD.

(C) Rosetta scores of glycosylated RBDs for normalized solvent accessible surface (SASA) and residue clash score (fa\_rep of sugar residues).

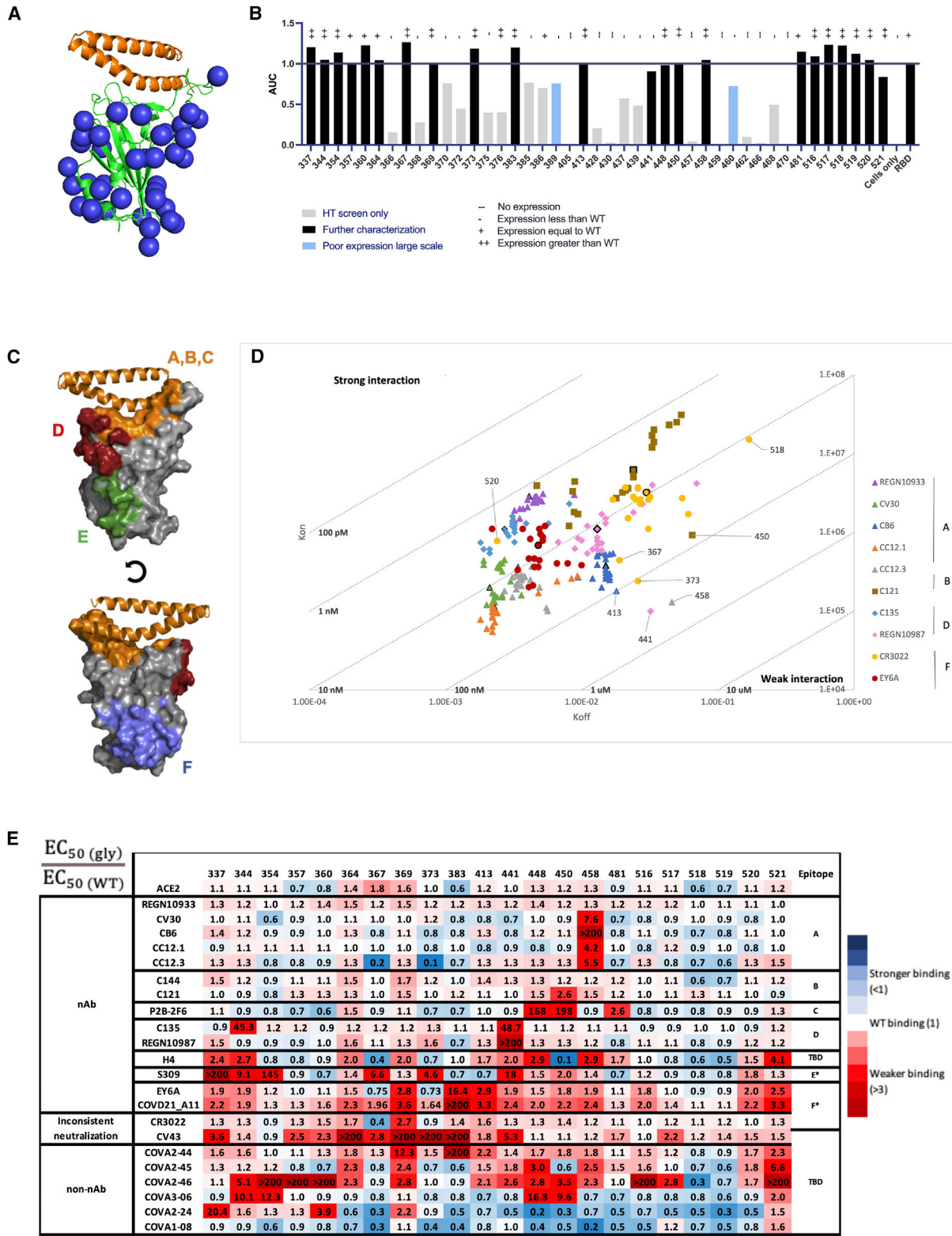
(D) Protein folding (total Rosetta score) versus glycan score (fa\_rep of sugar and protein) for each of the glycosylated RBDs selected in (C).

Selection criteria shown as dashed lines in (C and D).

### N-linked glycan decoration improves RBD-directed immunity

We utilized our single-glycan data to add sets of glycans to the RBD that maximally cover multiple non-neutralizing epitopes and preserve accessibility to RBS-targeted neutralizing epitopes. To this end, we constructed a glycan distance map allowing design of three, five, and eight glycan combinations that were experimentally tested to determine whether the sets could provide optimized antigenic profiles (Figures 3A and S1C–S1E). Two of the three glycan variants (g3.1 and g3.3) had heavily reduced binding to all antibodies in our panel. Eight glycan variants (g8.1, g8.2, and g8.3) had slightly reduced binding ( $EC_{50}$ ) to nearly all the RBD

nAbs (Figure 3B). However, both g3.2 and g5.1 (harboring three and five glycans, respectively) bound well to nAbs and had reduced affinity for non-nAbs (Figure 3B). Since new non-nAbs may be identified in the future, we focused the remaining experiments on the more glycosylated variants (i.e., g5.1 over g3.2), since they are more likely to reduce accessibility to epitopes recognized by non-nAbs. To determine the glycan composition of g5.1, we performed single-site glycan analysis by liquid chromatography-mass spectrometry (LC-MS) (Watanabe et al., 2020). To study the occupancy and processing states at each PNGS, we have determined the abundances of each glycan as oligomannose-type (high mannose,  $M_3\text{GlcNAc}_2$ – $M_9\text{GlcNAc}_2$ , including



(legend on next page)

glycosylated mannose); hybrid-type; complex-type divided in three subgroups, agalactosylated (contains no galactose), galactosylated (containing at least one galactose), and sialylated (containing at least one sialic acid); and unoccupied (no glycan). We also included core glycans in our analysis, which represents truncated glycan groups, i.e., compositions smaller than HexNAc(2)Hex(3). The N331, N343, N354, N428, and N481 show occupancy of galactosylated complex-type glycans, while N383 and N460 are unoccupied (Figure S1F). Interestingly, g5.1 has more occupied glycans than g8.2, suggesting g5.1 may be superior for focusing antibody responses (Figures S1F and S1G). To assess immune focusing of g5.1, we immunized BALB/c mice with a single 10- $\mu$ g injection of DNA plasmids encoding wild-type (WT) or g5.1 RBD (all immunizations in the manuscript are with DNA plasmids unless otherwise noted). In the immune-focused group (RBD g5.1), we observed higher titers of antibodies as assessed by area under the curve (AUC) analysis against both RBD and RBD g5.1 antigens (Figure 3C). The RBD-g5.1-immunized animals also produced higher titers of nAbs (Figure 3D). To investigate the difference in specificity of the RBD-elicited responses, we employed an ACE2-blocking assay (Walker et al., 2020; Figure 3E). We observed that RBD g5.1 elicited significantly more ACE2-blocking antibodies than WT RBD, suggesting g5.1 is immune-focusing antibodies to the RBS (Figures 3E and 3F). In a prime-boost experiment using a much larger 25- $\mu$ g dose, we observed similar immunogenicity between RBD groups but higher ACE2 blocking from animals immunized with the immune-focused RBD g5.1 (Figure S2). Together, these data demonstrate that combinations of strategically selected glycans reduce the affinity of non-nAbs and can focus immune responses to the neutralization-rich RBS or other epitopes of interest.

### DNA-launched nanovaccines amplify and accelerate immune responses

To develop multivalent vaccines, we genetically fused RBDs to a set of four different self-assembling scaffold proteins (Manolova et al., 2008; Kelly et al., 2019; Xu et al., 2020c; Zhao et al., 2014) with a potent CD4-helper epitope (LS-3) to help enhance germinal-center responses (Xu et al., 2020a). Tandem repeats of RBD have been shown to improve neutralization titers by 10- to 100-fold (Dai et al., 2020); thus, we displayed dimers of RBDs on some of our self-assembling scaffolds as well. We engineered nanoparticles using our computational design methods (Xu et al., 2020c), resulting in display of 7, 14, 24, 48, 60, 120, or 180 RBDs (Figure 4A). We rapidly screened 19 nanoparticles directly *in vivo* using a single mouse per construct at a single low dose of 2  $\mu$ g. We observed that 14 of the 19 nanoparticles were immunogenic (Figure 4B). Strikingly, rapid antibody responses were detected

just 1 week after immunization with RBD g5.1 24-mer, RBD 48-mer, and RBD g5.1 120-mer (Figure 4B). In parallel, we expressed and purified nanoparticles *in vitro*. In contrast to WT RBD multimers, which we could not purify and were not more immunogenic than RBD monomer when delivered as DNA (Figures S3A and S3B), we were able to purify nine glycan modified RBD multimers as assessed by size exclusion chromatography with multiangle light scattering (Figure 4C). To further confirm assembly of the RBD g5.1 24-mer, we employed structural analysis by cryoelectron microscopy (cryo-EM) for RBD g5.1 24-mer (Figures 4D, 4E, and S4B). Single-glycan analysis of RBD g5.1 24-mer shows similar occupancy to RBD g5.1 monomer; however, we observe full occupancy with highly processed-type glycans at N331 and N428 on the RBD g5.1 nanoparticle (Figure 4F). We conducted immunizations with selected constructs in BALB/c mice ( $n = 5$  or  $n = 10$ ) using a single low dose of 2  $\mu$ g (Figure 4G). At this single low dose, all the glycan-modified nanoparticle groups were more immunogenic than RBD or full-length S. RBD g5.1 24-mer and 120-mer both generated strong binding and neutralizing responses (week 4 mean inhibitory dose [ID<sub>50</sub>] of 3,677 and 791, respectively; Figures 4G and S3C). In C57BL/6 mice, we observed similar immunogenicity at 1  $\mu$ g and 5  $\mu$ g doses for select nanoparticles, including improvements in CD8<sup>+</sup> T cells (Figures S3H–S3K). RBD g8.2 7-mer and RBD g8.2 24-mer elicit similarly strong humoral responses when administered as purified protein nanoparticles (Figure S4A). Strikingly, we observed strong binding and neutralizing responses in BALB/c mice immunized with 5  $\mu$ g RBD g5.1 24-mer plasmid against the emergent B.1.17 (Alpha), B.1.351 (Beta), P.1 (Gamma), and B.1.617.2 (Delta) variants, indicating cross-reactivity and strong potential relevance against emerging variants (Figures 4H and S5A), unlike with a single dose of RBD monomer or full-length S (Figure S5C). As vaccine durability is a key parameter for prolonged protection, we monitored mice immunized with RBD g5.1 24-mer out past 6 months and observed maintenance of high neutralizing titers (Figure 4I). As proof of concept for expanding this platform to emerging variants, we engineered P.1/Gamma RBD g5.1 24-mer (Figure S5B). Upon BALB/c mice immunization with 2  $\mu$ g of P.1/Gamma RBD g5.1 24-mer, we observed high binding and cross-neutralization titers (Figures S3D and S3E).

### Single dose of RBD nanoparticles affords protection in lethal challenge model

To examine the efficacy of the SARS-CoV-2 RBD nanoparticles with rapid seroconversion (RBD g5.1 24-mer and RBD g5.1 120-mer), we pursued a lethal challenge study (Figure 5A). B6.Cg-Tg(K18-ACE2)2PrImn/J(K18-hACE2) mice express human ACE2 on epithelial cells, including in the airway (Chow

**Figure 2. *In vitro* characterization of single-glycan variants of RBD**

- (A) Model of selected glycan sites (blue spheres) on the RBD (green cartoon) interacting with ACE2-binding helices (orange cartoon).  
 (B) Small-scale screen of selected variants binding to ACE2 in area under the curve from ELISA binding curves and normalized to WT binding (bars); qualitative expression from western blot represented as +/- symbols above the bars.  
 (C) Neutralizing epitopes mapped on RBD structure with RBD in gray surface and ACE2-binding helices in orange; surface patches are colored as follows: RBD-A, -B, and -C are in orange; RBD-D is in red; RBD-E is in green; and RBD-F is in blue.  
 (D) SPR binding kinetics of single-glycan variants to a panel of SARS-CoV-2 antibodies.  
 (E) Relative binding as measured by ELISA EC<sub>50</sub> ratio of glycan variants binding to WT RBD binding in a panel of neutralizing and non-neutralizing antibodies. Blue to red coloring was done based on stronger or weaker binding relative to WT RBD.

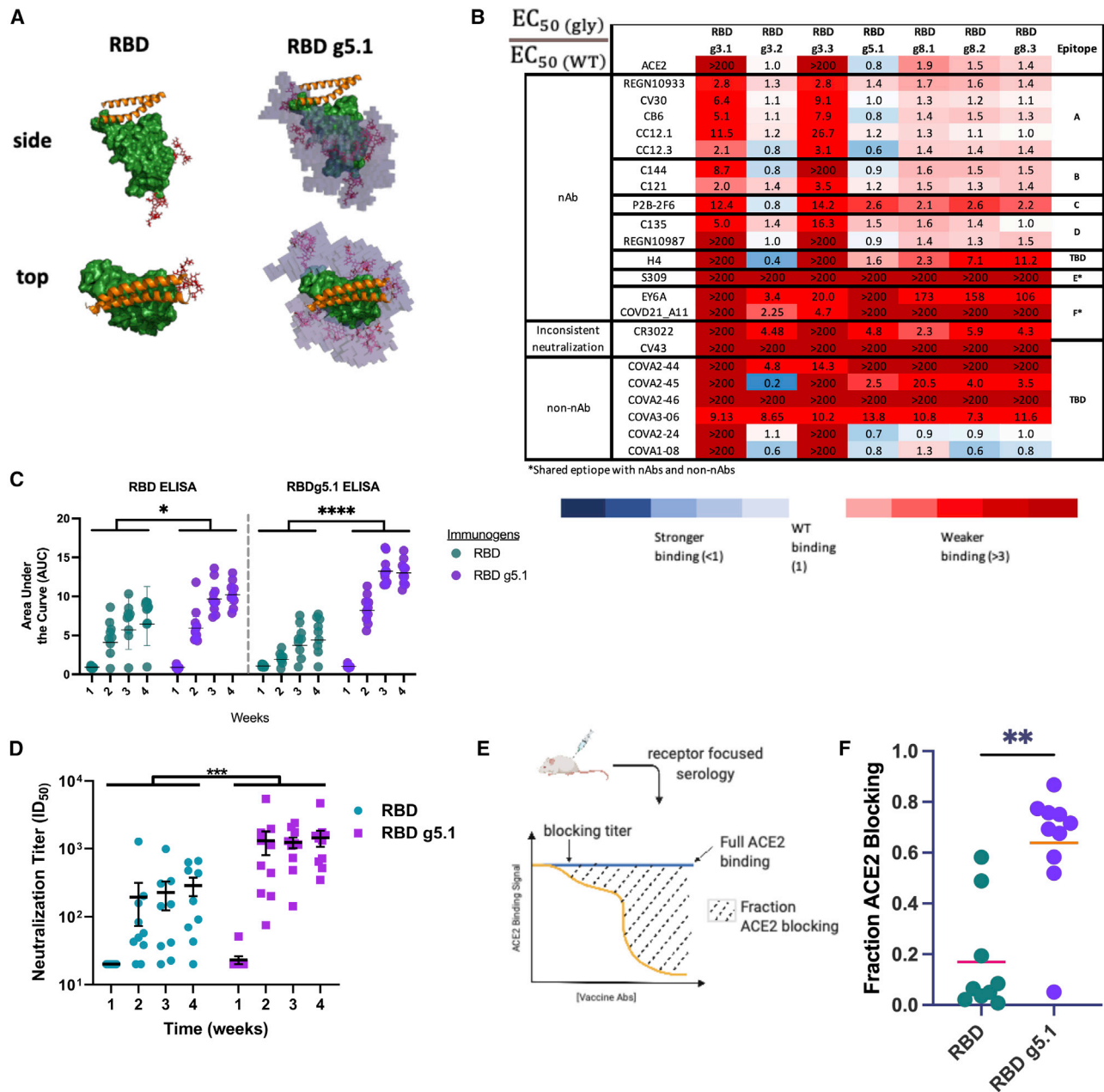


**Figure 3. In vitro and in vivo antigenic profile of multiglycan RBDs**

(A) Surface representation of RBD (green) bound to ACE2 (orange cartoons) with glycans (red sticks) for the WT RBD and RBD g5.1 constructs. Designed glycan voxels, or the space sampled by glycans, are depicted as purple blocks.

(B) Relative binding as measured by ELISA EC<sub>50</sub> ratio of glycan variants binding to a panel of neutralizing and non-neutralizing antibodies to WT RBD binding. Blue to red coloring was done based on stronger or weaker binding relative to WT RBD.

(C and D) Antibody binding titers (C) and pseudovirus ID<sub>50</sub> neutralization titers (D) from BALB/c mice immunized with 25 μg of plasmids encoding WT RBD or RBD g5.1 at weeks 0 and 2 (n = 10, duplicate).

(E) ACE2 competition assay layout for measuring blocking of ACE2 interacting with RBD with RBS-directed antibodies from the sera of vaccinated mice.

(F) Fraction of ACE2 binding blocked by antibodies in ACE2 competition assay (F) measured as the first dilution of sera at which a reduction in ACE2 binding is observed (unpaired two-tailed Student's t test; F, \*\*p = 0.0020; G, p = 0.0236; n = 10, duplicate).

et al., 1997, Mccray et al., 2007), and can be infected with SARS-CoV-2, resulting in weight loss and lethality (Oladunni et al., 2020), providing a stringent model for testing vaccines (Rathna-

singhe et al., 2020). Animals were vaccinated with a single shot of 5 μg and 1 μg of our nanovaccines in K18-ACE2 mice, representing doses 5- and 25-fold lower than our standard DNA dose



(Smith et al., 2020). Prior to a blinded challenge, we examined immunogenicity at day 21 and observed pseudovirus neutralization titers prior to challenge in all vaccine groups (Figure S6A). We also observed live SARS-CoV-2 virus neutralization titers above the limit of detection for all three nanoparticle groups with mean ID<sub>50</sub> of 451, 1,028, and 921 for RBD g5.1 120-mer 1 μg and 5 μg and RBD g5.1 24-mer 5 μg, respectively, compared with a mean ID<sub>50</sub> of 29 of RBD monomer (Figure 5B). The mice were infected with a high dose of SARS-CoV-2 1 × 10<sup>5</sup> plaque-forming units (PFUs)/mouse intranasally and monitored for signs of deteriorating health. We observed that mice immunized with nanovaccines had higher levels of protection from weight loss (Figure 5C). As expected, the naive group of animals reached 100% morbidity by day 6 and 1/10 animals survived in the RBD monomer group. Both RBD g5.1 120-mer groups had 6/10 mice survive the challenge. Strikingly, immunization with RBD g5.1 24-mer provided full protection from a lethal SARS-CoV-2 challenge (Figure 5D). All but one animal that survived had a live virus neutralization titer of >100, and 12/15 of the mice that succumbed to infection did not have appreciable neutralization titers (Figure 5E). We observed a significant correlation between live virus neutralization ID<sub>50</sub> titer and body weight loss (Figure 5F). Viral replication was absent in nasal turbinates, which may decrease viral transmissibility, and was reduced in lung tissue and brain tissue for mice immunized with nanovaccines relative to RBD monomer or naive animals (Figure 5G). Thus, the DNA-launched nanovaccines can generate potent immunity that provides protection from challenge with a single immunization at a low dose.

### Enhanced immune responses to nanovaccines in translational vaccine models

One major challenge for the clinical translation of vaccines is pre-clinical modeling of human antibody responses to immunogens. OmniMouse have humanized immunoglobulin loci transgenic

with human V, D, and J gene segments (Geurts et al., 2009). As a proof of concept, we immunized OmniMouse (n = 3) with three different SARS-CoV-2 nanoparticle vaccines (RBD 48-mer, RBD g5.1 24-mer, and RBD g8.3 60-mer) and measured increasing RBD-specific human antibodies in serum (Figures 6A and 6B). Most mice produced high titers of human immunoglobulin G (IgG), and a few had robust IgM titers (Figure S6B). We observed potent and specific neutralization in all three groups at weeks 6 and 8 (Figures 6C and S6C). Thus, the SARS-CoV-2 nanoparticle platform can be employed in transgenic mice and induce human SARS-CoV-2 nAbs.

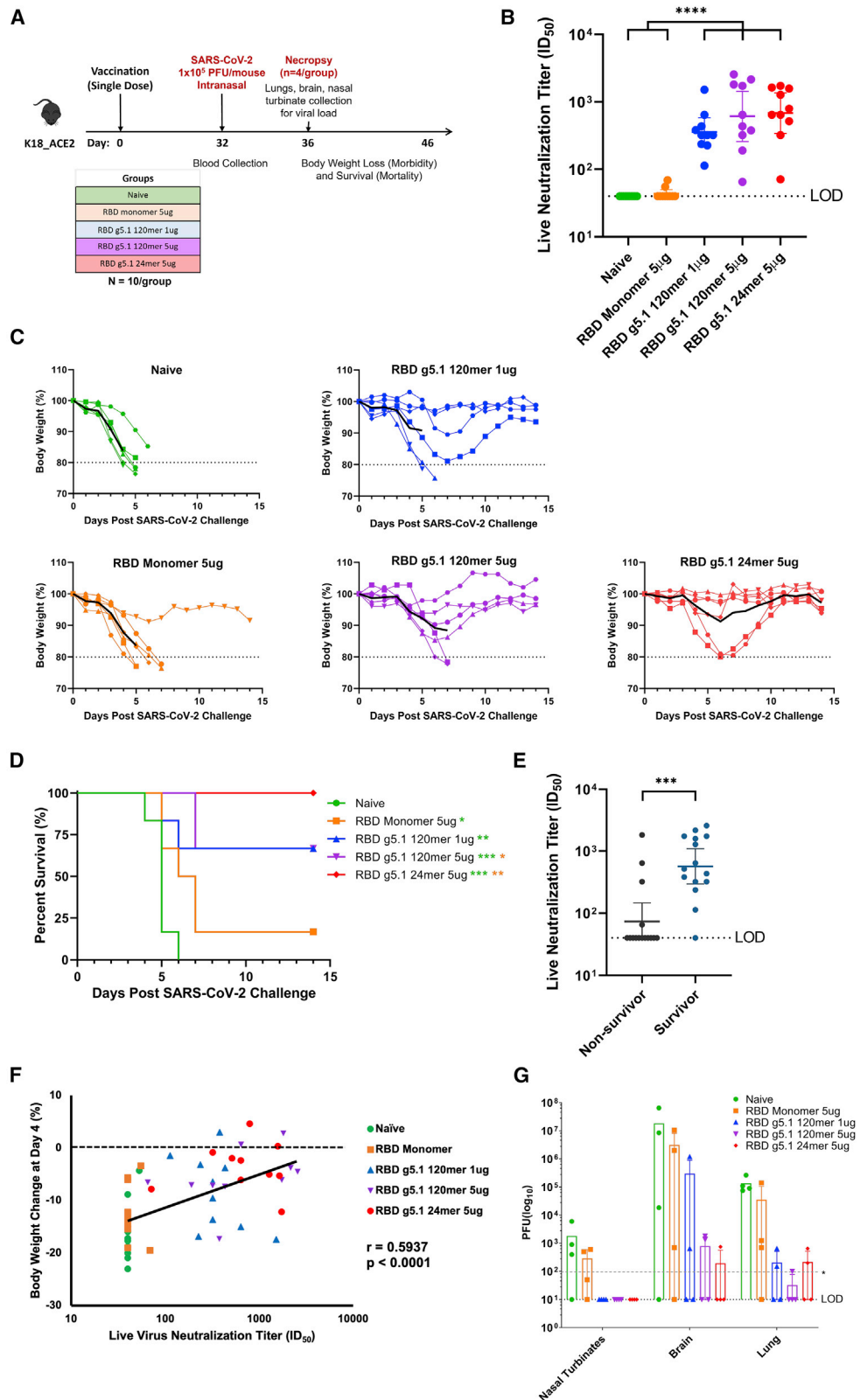
We assessed RBD g5.1 24-mer in Hartley guinea pigs (n = 6) to examine intradermal vaccine delivery at 0.5, 5, and 10 μg in comparison to RBD monomer at 10 μg. In contrast to the RBD-monomer-immunized group, we observed full seroconversion of RBD-g5.1-24-mer-immunized animals at a dose of 5 μg (Figure 6D). High levels of nAbs were obtained in the 10-μg-dose group (ID<sub>50</sub> of 1,840; Figure 6E). In a proof-of-concept study of RBD DLNPs prior to the development of RBD g5.1 24-mer, we immunized Syrian Golden hamsters (n = 5) twice 3 weeks apart with 2 μg and 10 μg of RBD monomer and RBD 48-mer (Figure 6F). The RBD-nanoparticle-immunized hamsters elicited higher antibody titers after both first and second doses and produced nAbs, unlike the responses in the RBD monomer vaccine groups (Figure 6G). To assess the biodistribution of anti-RBD IgG, we measured ultrafiltrated lung lavages and found antibodies only in the RBD nanoparticle groups (Figure 6H). In summary, we demonstrate that the DLNP vaccines provide enhanced immunogenicity in guinea pigs and hamsters.

### DISCUSSION

New SARS-CoV-2 vaccines should (1) alleviate cold chain requirements for global vaccine distribution, (2) improve immunogenicity

#### Figure 4. Immune-focused RBD nanoparticle structure and immunogenicity

- (A) Models of eight different RBD nanovaccines. In each model, the coloring is as follows: RBS (yellow) on the RBD (green) coated with glycans (blue) fused with a glycine-serine linker (gray) to a nanoparticle scaffold (red).
- (B) Endpoint titers for a single BALB/c mouse immunized once with 2 μg of plasmid-encoding RBD nanoparticles by DNA-E.P. colored as indicated on the figure; *in vitro* expression and assembly of nanoparticles indicated in the "ASM" column as either expressed/assembled (A), poor expression/assembly (X), or not tested (N).
- (C) Size-exclusion chromatogram (curves indicate UV absorbance and correspond to the left y axis) and multiangle light scattering data of RBD g5.1 multimers (black line under each curve indicates molecular weight and correspond to the right y axis).
- (D) 2D class averages showing RBDs decorating the RBD g5.1 24-mer.
- (E) cryo-EM density map of RBD g5.1 24-mer at low threshold; the 24-mer scaffold could be unambiguously determined (Figure S9), and the flexible linker attachment points for the RBDs on the 24-mer scaffold could be observed at low-density threshold (blue dots).
- (F) Glycan compositions at each potential N-linked glycan site (PNGS) are represented as bar graphs present in RBD g5.1 24-mer. Glycans were categorized and colored according to the detected compositions. Oligomannose-type glycans (M9–M4) are colored green. Hybrid-type glycans, those containing three HexNAcs and at least five hexoses, were colored as for complex-type glycans, because one arm can be processed in a similar manner. Complex-type glycans were categorized according to the number of HexNAc residues detected and the presence or absence of fucose. Core glycans represent any detected composition smaller than HexNAc<sub>2</sub>Hex<sub>3</sub>. For hybrid- and complex-type glycans, bars are colored to represent the terminal processing present. Blue represents agalactosylated, yellow galactosylated (containing at least one galactose), and purple sialylated (containing at least one sialic acid). The proportion of unoccupied PNGS is colored gray.
- (G) Endpoint titers for expanded groups (n = 5) of BALB/c mice immunized with 2 μg of plasmid encoding RBD nanoparticles by DNA-E.P.
- (H) Pseudovirus neutralization of SARS-CoV-2 variants B.1 (WT), B.1.351 (Beta), B.1.1.7 (Alpha), P.1 (Gamma), and B.1.617.2 (Delta) by sera from BALB/c mice immunized with 5 μg RBD g5.1 24-mer.
- (I) Pseudovirus neutralization of SARS-CoV-2 variants B.1 (WT), B.1.351 (Beta), B.1.1.7 (Alpha), P.1 (Gamma), and B.1.617.2 (Delta) over time. (G–I) n = 5, duplicate.



(legend on next page)

in the elderly and immunocompromised populations, (3) have increased efficacy when administered as a single dose or as a booster, and (4) protect against emerging variants that reduce or evade current vaccine-induced immunity. We have demonstrated that advanced DNA formulation and delivery technology coupled with immune-focused nanovaccines can provide a platform to address these translational obstacles for SARS-CoV-2 vaccines.

Viral glycan evolution results in antigenic changes with concomitant immune evasion. It has been observed that, for influenza, humoral immunity becomes restricted over time due to glycan additions (Altman et al., 2019). SARS-CoV-2 mutational variants may escape from antibody-mediated immunity. Glycan mutational variants may begin to circulate, given their large impact on antibody recognition of virus. Here, we provide a map of possible glycan additions to the RBD of SARS-CoV-2 and their effect on a large series of nAbs. Interestingly, we find a glycan at positions 458, 369, 450, and 441 can bind to human ACE2 but strongly reduces binding to nAbs targeting the sites RBD-A, -B, -C, and -D, respectively. Further, the glycan occupancy is an important parameter for immunogen design, as underoccupancy at glycan site has been shown to elicit non-nAbs (Cottrell et al., 2020; Derking et al., 2021). We show that addition of glycans to RBD-based nanovaccines can improve expression, assembly, immunogenicity, and neutralization.

The synthetic DNA platform employed in this study can be leveraged for generation of enhanced immunity, easier global distribution, and rapid reformulation. New adaptive electroporation systems can improve uptake of DNA plasmid up to 500 times (Gary and Weiner, 2020). In stark contrast to complex recombinant protein and RNA-based product development, DNA-based production and purification are extremely easy, due to availability of off-the-shelf commercial purification kits used widely in research laboratories. DNA vaccines are also much more chemically and thermally stable, allowing storage at room temperature for long periods of time. These characteristics of the DNA platform allow for new vaccines to be developed at breakneck speed and distributed to resource-limited settings around the globe.

A key finding in this study is the dose-sparing immunogenicity afforded by the nanoparticle designs. Most SARS-CoV-2 vaccines require at least two doses (Polack et al., 2020; Baden et al., 2021). DNA vaccines often require higher vaccine doses (25  $\mu$ g in mice, Smith et al., 2020, and 5 mg in non-human primates (NHPs), Yu et al., 2020) and/or advanced delivery devices

to drive sufficient immunogenicity. Here, we observed strong immunogenicity and protection from bona fide SARS-CoV-2 challenge down to 1  $\mu$ g. However, we did observe weight loss in 2/6 mice after challenge and low viral titers in 2/4 mice sacrificed 4 days after challenge. Increasing the dose to 10  $\mu$ g or by prime boosting could improve on our results. In fact, our studies of DNA-launched nanoparticle vaccines in guinea pigs and hamsters demonstrated greater immunogenicity than RBD monomer at a low dose of 10  $\mu$ g.

In comparison to other RBD nanoparticle systems, we have demonstrated significant improvements. Recently, studies on two-component S-based nanoparticle showed strong immunogenicity with sporadic pseudovirus neutralization 2 weeks post-prime (Brouwer et al., 2021; Walls et al., 2020). After two doses of the i53-50 RBD nanoparticle vaccine, mice challenged with  $1 \times 10^5$  PFUs of a mouse-adapted non-lethal virus were observed to have reduced viral replication (Walls et al., 2020). SpyTag-coupled RBD nanoparticles induce binding, but not nAbs, 2 weeks post-prime (Cohen et al., 2021; He et al., 2020; Zhang et al., 2020; Tan et al., 2021). An RBD-HR SpyTag nanoparticle was observed to induce immunity after two doses, which, after challenge with  $4 \times 10^4$  PFUs authentic SARS-CoV-2, could reduce viral load in the lungs (Ma et al., 2020). Here, the DNA-launched, glycan-modified RBDs could be genetically fused with four different nanoparticles scaffolds; the simple genetic fusion results in a single vaccine product that could induce binding and nAbs 1 week post-prime immunization and induce CD8<sup>+</sup> T cells. We created a more stringent test of immunity than most previous studies, as we used authentic SARS-CoV-2 virus with 2.5-fold higher amount of virus ( $1 \times 10^5$  PFUs) in the challenge and a 10-fold more sensitive viral detection assay. Further, vaccines studied in this model mostly utilize a prime and boost to achieve protection. In this model, our nanovaccines could induce immunity that reduced viral replication and completely protected from death at a low single dose of 5  $\mu$ g. From the data, there is an 82% chance of survival if mice have a live virus neutralization titer >100 prior to challenge. Given the protective threshold for nAbs that we observe, we expect that the high levels of cross-reactivity neutralization to the B.1.1.7 (Alpha), B.1.351 (Beta), P.1 (Gamma), B.1.617.2 (Delta), and B.1.1.529 (Omicron) SARS-CoV-2 variants that can be generated by our nanovaccine would protect in a similar lethal challenge. In addition, the P.1/Gamma RBD g5.1 nanoparticle elicited high levels of cross-reactive antibodies that could be employed as a booster vaccine.

#### Figure 5. Lethal challenge of SARS-CoV-2 in rodent model

- (A) K18 hACE2 lethal challenge study overview.  
 (B) SARS-CoV-2 live virus neutralization 1 day prior to challenge. \*\*\*\*p < 0.0001.  
 (C) Weight loss of K18 hACE2 mice after SARS-CoV-2 challenge.  
 (D) Kaplan-Meier curves representing survival of K18 hACE2 mice after SARS-CoV-2 challenge (Mantel-Cox test versus naive: RBD monomer \*p = 0.0327, RBD g5.1 24-mer p = 0.0006, \*\*RBD g5.1 120-mer 1  $\mu$ g p = 0.0087, RBD g5.1 120-mer 5  $\mu$ g p = 0.0006; versus RBD monomer: \*\*\* RBD g5.1 120-mer 5  $\mu$ g p = 0.0426, \*\*\* RBD g5.1 24-mer p = 0.0048; n = 6).  
 (E) Pseudovirus neutralization titers of surviving and non-surviving mice (unpaired, two-tailed Student's t test; \*\*\*p = 0.0003).  
 (F) Correlation between body weight change at day 4 post-challenge and pre-challenge live virus neutralizing titers (ID<sub>50</sub>).  
 (G) Viral titers in nasal turbinates and brain and lung tissue at day 4 post-challenge (unpaired, two-tailed Student's t test versus naive: RBD 120-mer 1  $\mu$ g p = 0.0110, RBD 120-mer 5  $\mu$ g p = 0.0109, RBD g5.1 24-mer p = 0.0110; n = 4, duplicate). LOD for this assay (lower dashed line) is lower than the LOD reported elsewhere (top dashed line).

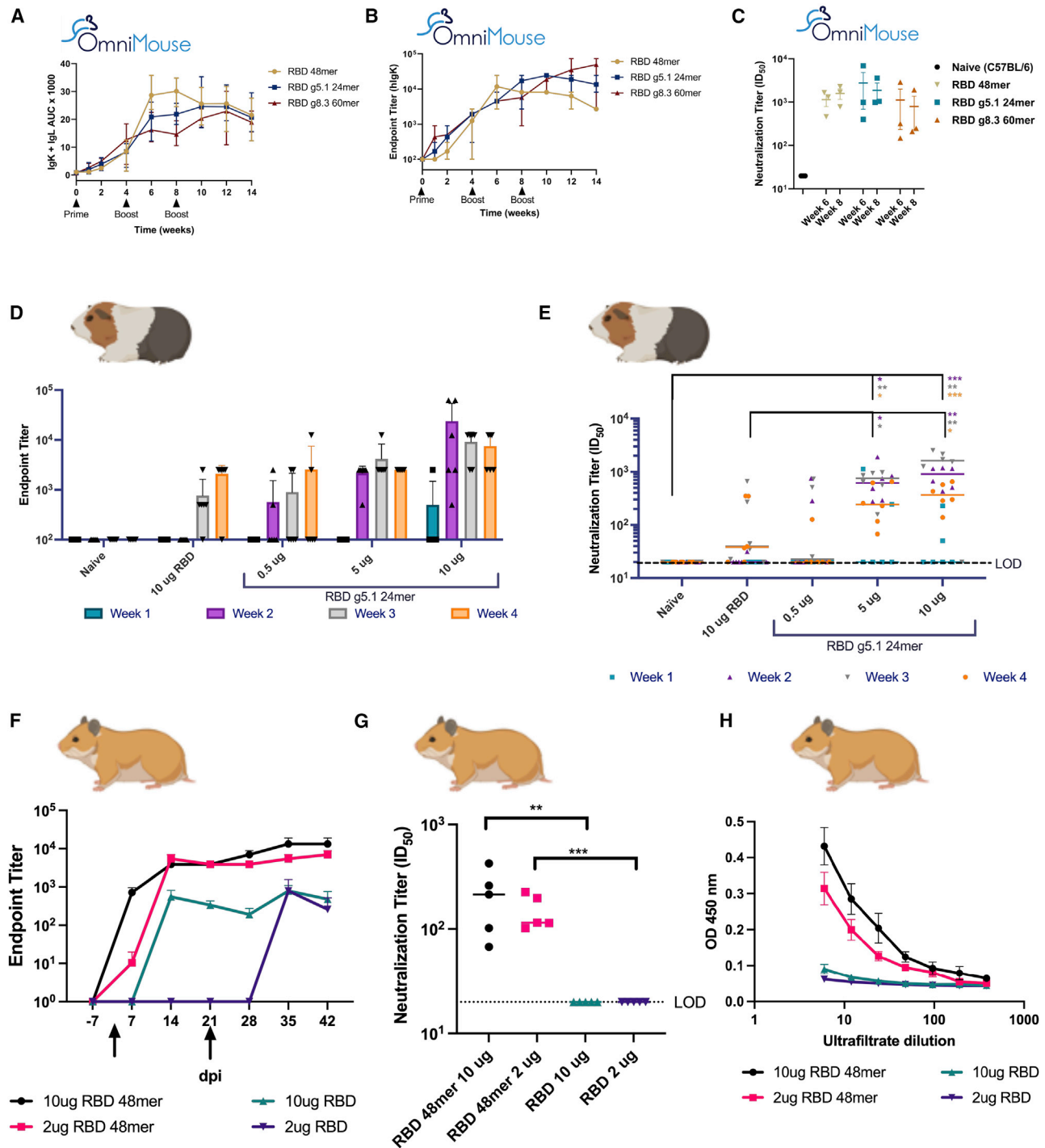


**Figure 6. Humoral responses to nanovaccines in OmniMouse, guinea pigs, and hamsters**

(A) Human antibody titers from OmniMouse (n = 3, duplicate) immunized three times 4 weeks apart with 25 µg of DNA-encoding RBD nanoparticles as measured by combined AUC from ELISA curves with human IgK and human IgL secondaries (the error bars represent mean and range).

(B) Same as (A) as measured by endpoint titer using human IgK and human IgL secondaries (the error bars represent mean and range).

(C) Pseudo-virus neutralization titers at week 6 and week 8 post-immunization (the error bars represent mean and SD).

(D) Endpoint titers against RBD for sera from Hartley guinea pigs immunized with RBD monomer and RBD g5.1 24-mer after a single dose (the error bars represent mean and SD).

(E) Pseudo-virus neutralization of sera from guinea pigs (n = 6, duplicate) immunized with RBD monomer and RBD g5.1 24-mer after a single dose (unpaired t test versus naive: 5 µg RBD g5.1 24-mer week 2 \*p = 0.0140, week 3 \*\*p = 0.0003, \*week 4 p = 0.0146; 10 µg RBD g5.1 24-mer: week 2 \*\*\*p = 0.0145, week

(legend continued on next page)

In conclusion, we have developed a single-dose SARS-CoV-2 nanovaccine with a platform that can afford rapid pre-clinical re-configuration to address variants of concern and for clinical translation.

### Limitations of the study

A potential limitation of our approach is that, while the addition of glycans to vaccine immunogens can prevent induction of non-nAbs and enrich for nAbs, glycans may also alter other antibody binding, which may be important. As with all *in vivo* antigen-generating platforms, including DNA, tissue expression may have effects on glycan structure due to differences in enzymatic availability. Additional studies following up on glycosylation differences of *in vivo* and *in vitro* immunogens are warranted.

### STAR★METHODS

Detailed methods are provided in the online version of this paper and include the following:

- KEY RESOURCES TABLE
- RESOURCE AVAILABILITY
  - Lead contact
  - Materials availability
  - Data and code availability
- EXPERIMENTAL MODEL AND SUBJECT DETAILS
  - Animals
  - Cell lines
- METHOD DETAILS
  - Cloaking with glycans algorithm
  - Nanoparticle modeling
  - Protein expression and purification
  - Western Blot
  - ELISA
  - Surface plasmon resonance
  - Pseudovirus neutralization assay
  - SARS-CoV-2 culture, titer, and neutralization assay
  - Animal studies
  - Hamster biodistribution
  - Negative-stain electron microscopy
  - Cryo electron microscopy
  - ELISpot assay
  - Intracellular cytokine staining and flow cytometry
  - Competition assay
  - Site-specific glycan analysis using mass spectrometry
- QUANTIFICATION AND STATISTICAL ANALYSIS

### SUPPLEMENTAL INFORMATION

Supplemental information can be found online at <https://doi.org/10.1016/j.celrep.2022.110318>.

### ACKNOWLEDGMENTS

The authors would like to thank the Wistar Institute Core facilities for providing care to the animals. We would like to acknowledge Dr. Jason S. McLellan for providing reagents for hamster serology. We would also like to thank Dr. Jared Adolf-Bryfogle for generously contributing GTM code to Rosetta for use in this project. This research, including design of nanoparticles, was supported by Wistar Coronavirus Discovery Fund, a CURE/PA Department of Health grant (SAP no. 4100083104), and a COVID/PA Department of Human Services grant (SAP no. 4100089371) awarded to D.W.K. The DNA immunizations were supported by NIH/NIAID CIVICs (75N93019C00051), Wistar Coronavirus Discovery Fund, Wistar SRA 16-4/Inovio Pharmaceuticals, and COVID/PA Department of Human Services (SAP no. 4100089371) awarded to D.B.W. This research was supported by Indiana University start-up funds to J.P. The funding sources were not involved in the design of this study, collection and analyses of data, or decision to submit the manuscript.

### AUTHOR CONTRIBUTIONS

K.M.K., Y.W., and D.W.K. designed immunogens. K.M.K., K.L., Z.X., S.N.W., X.Z., N.C., N.J.T., M.P., J.P., E.L.R., D.F., C.I., A.P., D.B.W., and D.W.K. planned experiments. K.M.K., K.L., Z.X., S.N.W., X.Z., N.C., N.J.T., M.P., J.P., J.D., A.M., B.F., E.L.R., and D.F. conducted experiments. K.S., K.E.B., L.M.P.F.H., and T.R.F.S. contributed resources for lethal challenge study. C.I. contributed resources for the human antibody transgenic mouse study. K.M.K., K.L., Z.X., S.N.W., X.Z., N.C., N.J.T., M.P., J.P., E.L.R., J.D., A.M., D.F., and D.W.K. analyzed the data. K.M.K. and D.W.K. wrote the article. K.M.K., K.L., Y.W., S.N.W., N.C., J.D., A.M., J.P., D.B.W., and D.W.K. edited the article.

### DECLARATION OF INTERESTS

T.R.F.S., K.S., K.E.B., and L.M.P.F.H. are employees of Inovio Pharmaceuticals and as such receive salary and benefits, including ownership of stock and stock options, from the company. C.I. is an employee of Ligand Pharmaceuticals, Inc. and as such receives salary and benefits from the company. D.W.K. reports a patent for nanoparticle vaccine pending. D.B.W. has received grant funding, participates in industry collaborations, has received speaking honoraria, and has received fees for consulting, including serving on scientific review committees and board services. Remuneration received by D.B.W. includes direct payments or stock or stock options, and in the interest of disclosure, he notes potential conflicts associated with this work with Inovio Pharmaceuticals and possibly others. In addition, he has a patent DNA vaccine delivery pending to Inovio Pharmaceuticals. The other authors declare no competing interests.

Received: May 24, 2021

Revised: October 18, 2021

Accepted: January 7, 2022

Published: January 10, 2022

### REFERENCES

Altman, M.O., Angel, M., Kosik, I., Trovao, N.S., Zost, S.J., Gibbs, J.S., Casalino, L., Amaro, R.E., Hensley, S.E., Nelson, M.I., and Yewdell, J.W. (2019). Human influenza A virus hemagglutinin glycan evolution follows a temporal pattern to a glycan limit. *mBio* 10, 1–15.

3 \*\*p = 0.0016, week 4 \*\*\*p = 0.0007. Unpaired t test versus 10 μg RBD to 5 μg RBD g5. 1 24-mer week 2 \*p = 0.0142, week 3 \*p = 0.0104; 10 μg RBD g5. 1 24-mer week 2 \*\*p = 0.0002, week 3 \*\*p = 0.0042, week 4 \*p = 0.0304.

(F) Endpoint-binding titers against RBD for sera from Syrian Golden hamsters (n = 5, duplicate) immunized with RBD monomer or RBD 48-mer two times with two different doses (the error bars represent mean and SD).

(G) Neutralization of SARS-CoV-2 pseudovirus by sera from hamsters immunized with RBD monomer or RBD 48-mer with two different doses (unpaired, two-tailed Student's t test: RBD 48-mer 10 μg versus RBD monomer 10 μg \*\*p = 0.0079; RBD 48-mer 2 μg versus RBD monomer 2 μg \*\*\*p = 0.0004).

(H) Lung lavages from hamsters immunized with RBD monomer or RBD 48-mer (the error bars represent mean and SD).

- Baden, L.R., El Sahly, H.M., Essink, B., Kotloff, K., Frey, S., Novak, R., Diemert, D., Spector, S.A., Roupael, N., Creech, C.B., et al. (2021). Efficacy and safety of the mRNA-1273 SARS-CoV-2 vaccine. *N. Engl. J. Med.* **384**, 403–416.
- Bajic, G., Maron, M.J., Adachi, Y., Onodera, T., Mccarthy, K.R., Mcgee, C.E., Sempowski, G.D., Takahashi, Y., Kelsoe, G., Kuraoka, M., and Schmidt, A.G. (2019). Influenza antigen engineering focuses immune responses to a sub-dominant but broadly protective viral epitope. *Cell Host Microbe* **25**, 827–835 e6.
- Barnes, C.O., Jette, C.A., Abernathy, M.E., Dam, K.A., Esswein, S.R., Gristick, H.B., Maljutin, A.G., Sharaf, N.G., Huey-Tubman, K.E., Lee, Y.E., et al. (2020). SARS-CoV-2 neutralizing antibody structures inform therapeutic strategies. *Nature* **588**, 682–687.
- Brouwer, P.J.M., Brinkkemper, M., Maisonnasse, P., Dereuddre-Bosquet, N., Grobden, M., Claireaux, M., De Gast, M., Marlin, R., Chesnais, V., Diry, S., et al. (2021). Two-component spike nanoparticle vaccine protects macaques from SARS-CoV-2 infection. *Cell* **184**, 1188–1200 e19.
- Brouwer, P.J.M., Caniels, T.G., Van Der Straten, K., Snitselaar, J.L., Aldon, Y., Bangaru, S., Torres, J.L., Okba, N.M.A., Claireaux, M., Kerster, G., et al. (2020). Potent neutralizing antibodies from COVID-19 patients define multiple targets of vulnerability. *Science* **369**, 643–650.
- Byrnes, J.R., Zhou, X.X., Lui, I., Elledge, S.K., Glasgow, J.E., Lim, S.A., Loudermilk, R.P., Chiu, C.Y., Wang, T.T., Wilson, M.R., et al. (2020). Competitive SARS-CoV-2 serology reveals most antibodies targeting the spike receptor-binding domain compete for ACE2 binding. *mSphere* **5**, e00802-20.
- Chow, Y.H., O'brodovich, H., Plumb, J., Wen, Y., Sohn, K.J., Lu, Z., Zhang, F., Lukacs, G.L., Tanswell, A.K., Hui, C.C., et al. (1997). Development of an epithelium-specific expression cassette with human DNA regulatory elements for transgene expression in lung airways. *Proc. Natl. Acad. Sci. U S A* **94**, 14695–14700.
- Cohen, A.A., Gnanapragasam, P.N.P., Lee, Y.E., Hoffman, P.R., Ou, S., Kakutani, L.M., Keeffe, J.R., Wu, H.J., Howarth, M., West, A.P., et al. (2021). Mosaic nanoparticles elicit cross-reactive immune responses to zoonotic coronaviruses in mice. *Science* **371**, 735–741.
- Cottrell, C.A., Van Schooten, J., Bowman, C.A., Yuan, M., Oyen, D., Shin, M., Morpurgo, R., Van Der Woude, P., Van Breemen, M., Torres, J.L., et al. (2020). Mapping the immunogenic landscape of near-native HIV-1 envelope trimers in non-human primates. *PLoS Pathog.* **16**, e1008753.
- Dai, L., Zheng, T., Xu, K., Han, Y., Xu, L., Huang, E., An, Y., Cheng, Y., Li, S., Liu, M., et al. (2020). A universal design of betacoronavirus vaccines against COVID-19, MERS, and SARS. *Cell* **182**, 722–733 e11.
- De Taeye, S.W., De La Pena, A.T., Vecchione, A., Scutigliani, E., Sliopen, K., Burger, J.A., Van Der Woude, P., Schorcht, A., Schermer, E.E., Van Gils, M.J., et al. (2018). Stabilization of the gp120 V3 loop through hydrophobic interactions reduces the immunodominant V3-directed non-neutralizing response to HIV-1 envelope trimers. *J. Biol. Chem.* **293**, 1688–1701.
- Derking, R., Allen, J.D., Cottrell, C.A., Sliopen, K., Seabright, G.E., Lee, W.H., Aldon, Y., Rantalainen, K., Antanasijevic, A., Copps, J., et al. (2021). Enhancing glycan occupancy of soluble HIV-1 envelope trimers to mimic the native viral spike. *Cell Rep.* **35**, 108933.
- Dong, E., Du, H., and Gardner, L. (2020). An interactive web-based dashboard to track COVID-19 in real time. *Lancet Infect. Dis.* **20**, 533–534.
- Du, L., Tai, W., Yang, Y., Zhao, G., Zhu, Q., Sun, S., Liu, C., Tao, X., Tseng, C.K., Perlman, S., et al. (2016). Introduction of neutralizing immunogenicity index to the rational design of MERS coronavirus subunit vaccines. *Nat. Commun.* **7**, 13473.
- Elbe, S., and Buckland-Merrett, G. (2017). Data, disease and diplomacy: GISAID's innovative contribution to global health. *Glob. Chall.* **1**, 33–46.
- Gary, E.N., and Weiner, D.B. (2020). DNA vaccines: prime time is now. *Curr. Opin. Immunol.* **65**, 21–27.
- Geurts, A.M., Cost, G.J., Freyvert, Y., Zeittler, B., Miller, J.C., Choi, V.M., Jenkins, S.S., Wood, A., Cui, X., Meng, X., et al. (2009). Knockout rats via embryo microinjection of zinc-finger nucleases. *Science* **325**, 433.
- Hansen, J., Baum, A., Pascal, K.E., Russo, V., Giordano, S., Wloga, E., Fulton, B.O., Yan, Y., Koon, K., Patel, K., et al. (2020). Studies in humanized mice and convalescent humans yield a SARS-CoV-2 antibody cocktail. *Science* **369**, 1010–1014.
- Hariharan, V., and Kane, R.S. (2020). Glycosylation as a tool for rational vaccine design. *Biotechnol. Bioeng.* **117**, 2556–2570.
- He, L., Lin, X., Wang, Y., Abraham, C., Sou, C., Ngo, T., Zhang, Y., Wilson, I.A., and Zhu, J. (2020). Self-assembling nanoparticles presenting receptor binding domain and stabilized spike as next-generation COVID-19 vaccines. *bioRxiv*, 1–33.
- Huo, J., Zhao, Y., Ren, J., Zhou, D., Duyvesteyn, H.M.E., Ginn, H.M., Carrique, L., Malinauskas, T., Ruza, R.R., Shah, P.N.M., et al. (2020). Neutralization of SARS-CoV-2 by destruction of the prefusion spike. *Cell Host Microbe* **28**, 497.
- Impagliazzo, A., Milder, F., Kuipers, H., Wagner, M.V., Zhu, X., Hoffman, R.M., Van Meersbergen, R., Huizingh, J., Wanningen, P., Verspuij, J., et al. (2015). A stable trimeric influenza hemagglutinin stem as a broadly protective immunogen. *Science* **349**, 1301–1306.
- Ingale, J., Tran, K., Kong, L., Dey, B., Mckee, K., Schief, W., Kwong, P.D., Mascola, J.R., and Wyatt, R.T. (2014). Hyperglycosylated stable core immunogens designed to present the CD4 binding site are preferentially recognized by broadly neutralizing antibodies. *J. Virol.* **88**, 14002–14016.
- Ju, B., Zhang, Q., Ge, J., Wang, R., Sun, J., Ge, X., Yu, J., Shan, S., Zhou, B., Song, S., et al. (2020). Human neutralizing antibodies elicited by SARS-CoV-2 infection. *Nature* **584**, 115–119.
- Kelly, H.G., Kent, S.J., and Wheatley, A.K. (2019). Immunological basis for enhanced immunity of nanoparticle vaccines. *Expert Rev. Vaccines* **18**, 269–280.
- Krammer, F., and Palese, P. (2013). Influenza virus hemagglutinin stalk-based antibodies and vaccines. *Curr. Opin. Virol.* **3**, 521–530.
- Kulp, D.W., Steichen, J.M., Pauthner, M., Hu, X., Schiffner, T., Liguori, A., Cottrell, C.A., Havenar-Daughton, C., Ozorowski, G., Georgeson, E., et al. (2017). Structure-based design of native-like HIV-1 envelope trimers to silence non-neutralizing epitopes and eliminate CD4 binding. *Nat. Commun.* **8**, 1655.
- Lee, W.S., Wheatley, A.K., Kent, S.J., and Dekosky, B.J. (2020). Antibody-dependent enhancement and SARS-CoV-2 vaccines and therapies. *Nat. Microbiol.* **5**, 1185–1191.
- Lei, C., Yang, J., Hu, J., and Sun, X. (2021). On the calculation of TCID<sub>50</sub> for quantitation of virus infectivity. *Virol. Sin* **36**, 141–144.
- Letko, M., Marzi, A., and Munster, V. (2020). Functional assessment of cell entry and receptor usage for SARS-CoV-2 and other lineage B betacoronaviruses. *Nat. Microbiol.* **5**, 562–569.
- Liu, L., Wang, P., Nair, M.S., Yu, J., Rapp, M., Wang, Q., Luo, Y., Chan, J.F., Sahi, V., Figueroa, A., et al. (2020). Potent neutralizing antibodies against multiple epitopes on SARS-CoV-2 spike. *Nature* **584**, 450–456.
- Ly, A., and Stamatatos, L. (2000). V2 loop glycosylation of the human immunodeficiency virus type 1 SF162 envelope facilitates interaction of this protein with CD4 and CCR5 receptors and protects the virus from neutralization by anti-V3 loop and anti-CD4 binding site antibodies. *J. Virol.* **74**, 6769–6776.
- Ma, X., Zou, F., Yu, F., Li, R., Yuan, Y., Zhang, Y., Zhang, X., Deng, J., Chen, T., Song, Z., et al. (2020). Nanoparticle vaccines based on the receptor binding domain (RBD) and heptad repeat (HR) of SARS-CoV-2 elicit robust protective immune responses. *Immunity* **53**, 1315–1330 e9.
- Manolova, V., Flace, A., Bauer, M., Schwarz, K., Saudan, P., and Bachmann, M.F. (2008). Nanoparticles target distinct dendritic cell populations according to their size. *Eur. J. Immunol.* **38**, 1404–1413.
- Mccray, P.B., Jr., Pewe, L., Wohlford-Lenane, C., Hickey, M., Manzel, L., Shi, L., Netland, J., Jia, H.P., Halabi, C., Sigmund, C.D., et al. (2007). Lethal infection of K18-hACE2 mice infected with severe acute respiratory syndrome coronavirus. *J. Virol.* **81**, 813–821.
- Medina, R.A., Stertz, S., Manicassamy, B., Zimmermann, P., Sun, X., Albrecht, R.A., Uusi-Kerttula, H., Zagordi, O., Belshe, R.B., Frey, S.E., et al. (2013). Glycosylations in the globular head of the hemagglutinin protein modulate the

- virulence and antigenic properties of the H1N1 influenza viruses. *Sci. Transl. Med.* **5**, 187ra70.
- Oladunni, F.S., Park, J.G., Pino, P.A., Gonzalez, O., Akhter, A., Allue-Guardia, A., Olmo-Fontanez, A., Gautam, S., Garcia-Vilanova, A., Ye, C., et al. (2020). Lethality of SARS-CoV-2 infection in K18 human angiotensin-converting enzyme 2 transgenic mice. *Nat. Commun.* **11**, 6122.
- Piccoli, L., Park, Y.J., Tortorici, M.A., Czudnochowski, N., Walls, A.C., Beltramello, M., Silacci-Fregni, C., Pinto, D., Rosen, L.E., Bowen, J.E., et al. (2020). Mapping neutralizing and immunodominant sites on the SARS-CoV-2 spike receptor-binding domain by structure-guided high-resolution serology. *Cell* **183**, 1024–1042 e21.
- Pinto, D., Park, Y.J., Beltramello, M., Walls, A.C., Tortorici, M.A., Bianchi, S., Jaconi, S., Culp, K., Zatta, F., De Marco, A., et al. (2020). Cross-neutralization of SARS-CoV-2 by a human monoclonal SARS-CoV antibody. *Nature* **583**, 290–295.
- Polack, F.P., Thomas, S.J., Kitchin, N., Absalon, J., Gurtman, A., Lockhart, S., Perez, J.L., Perez Marc, G., Moreira, E.D., Zerbini, C., et al. (2020). Safety and efficacy of the BNT162b2 mRNA covid-19 vaccine. *N. Engl. J. Med.* **383**, 2603–2615.
- Rathnasinghe, R., Strohmeier, S., Amanat, F., Gillespie, V.L., Krammer, F., Garcia-Sastre, A., Coughlan, L., Schotsaert, M., and Uccellini, M.B. (2020). Comparison of transgenic and adenovirus hACE2 mouse models for SARS-CoV-2 infection. *Emerg. Microbes Infect.* **9**, 2433–2445.
- Raybould, M.I.J., Kovaltsuk, A., Marks, C., and Deane, C.M. (2020). CoV-Ab-Dab: the coronavirus antibody database. *Bioinformatics* **37**, 734–735.
- Ren, H., and Zhou, P. (2016). Epitope-focused vaccine design against influenza A and B viruses. *Curr. Opin. Immunol.* **42**, 83–90.
- Robbiani, D.F., Gaebler, C., Muecksch, F., Lorenzi, J.C.C., Wang, Z., Cho, A., Agudelo, M., Barnes, C.O., Gazumyan, A., Finkin, S., et al. (2020). Convergent antibody responses to SARS-CoV-2 in convalescent individuals. *Nature* **584**, 437–442.
- Rogers, T.F., Zhao, F., Huang, D., Beutler, N., Burns, A., He, W.T., Limbo, O., Smith, C., Song, G., Woehl, J., et al. (2020). Isolation of potent SARS-CoV-2 neutralizing antibodies and protection from disease in a small animal model. *Science* **369**, 956–963.
- Rohou, A., and Grigorieff, N. (2015). CTFIND4: fast and accurate defocus estimation from electron micrographs. *J. Struct. Biol.* **192**, 216–221.
- Sanders, R.W., Derking, R., Cupo, A., Julien, J.P., Yasmeen, A., De Val, N., Kim, H.J., Blattner, C., De La Pena, A.T., Korzun, J., et al. (2013). A next-generation cleaved, soluble HIV-1 Env trimer, BG505 SOSIP.664 gp140, expresses multiple epitopes for broadly neutralizing but not non-neutralizing antibodies. *PLoS Pathog* **9**, e1003618.
- Scheres, S.H. (2012). A Bayesian view on cryo-EM structure determination. *J. Mol. Biol.* **415**, 406–418.
- Seydoux, E., Homad, L.J., Maccamy, A.J., Parks, K.R., Hurlburt, N.K., Jennewein, M.F., Akins, N.R., Stuart, A.B., Wan, Y.H., Feng, J., et al. (2020). Analysis of a SARS-CoV-2-infected individual reveals development of potent neutralizing antibodies with limited somatic mutation. *Immunity* **53**, 98–105 e5.
- Shi, R., Shan, C., Duan, X., Chen, Z., Liu, P., Song, J., Song, T., Bi, X., Han, C., Wu, L., et al. (2020). A human neutralizing antibody targets the receptor-binding site of SARS-CoV-2. *Nature* **584**, 120–124.
- Shinnakasu, R., Sakakibara, S., Yamamoto, H., Wang, P.H., Moriyama, S., Sax, N., Ono, C., Yamanaka, A., Adachi, Y., Onodera, T., et al. (2021). Glycan engineering of the SARS-CoV-2 receptor-binding domain elicits cross-neutralizing antibodies for SARS-related viruses. *J. Exp. Med.* **218**, e20211003.
- Smith, T.R.F., Patel, A., Ramos, S., Elwood, D., Zhu, X., Yan, J., Gary, E.N., Walker, S.N., Schultheis, K., Purwar, M., et al. (2020). Immunogenicity of a DNA vaccine candidate for COVID-19. *Nat. Commun.* **11**, 2601.
- Suthar, M.S., Zimmerman, M.G., Kauffman, R.C., Mantus, G., Linderman, S.L., Hudson, W.H., Vanderheiden, A., Nyhoff, L., Davis, C.W., Adekunle, O., et al. (2020). Rapid generation of neutralizing antibody responses in COVID-19 patients. *Cell Rep. Med.* **1**, 100040.
- Tan, T.K., Rijal, P., Rahikainen, R., Keeble, A.H., Schimanski, L., Hussain, S., Harvey, R., Hayes, J.W.P., Edwards, J.C., Mclean, R.K., et al. (2021). A COVID-19 vaccine candidate using SpyCatcher multimerization of the SARS-CoV-2 spike protein receptor-binding domain induces potent neutralizing antibody responses. *Nat. Commun.* **12**, 542.
- Tian, X., Li, C., Huang, A., Xia, S., Lu, S., Shi, Z., Lu, L., Jiang, S., Yang, Z., Wu, Y., and Ying, T. (2020). Potent binding of 2019 novel coronavirus spike protein by a SARS coronavirus-specific human monoclonal antibody. *Emerg. Microbes Infect.* **9**, 382–385.
- Wajnberg, A., Amanat, F., Firpo, A., Altman, D.R., Bailey, M.J., Mansour, M., McMahon, M., Meade, P., Mendu, D.R., Muellers, K., et al. (2020). Robust neutralizing antibodies to SARS-CoV-2 infection persist for months. *Science* **370**, 1227–1230.
- Walker, S.N., Chokkalingam, N., Reuschel, E.L., Purwar, M., Xu, Z., Gary, E.N., Kim, K.Y., Helble, M., Schultheis, K., Walters, J., et al. (2020). SARS-CoV-2 assays to detect functional antibody responses that block ACE2 recognition in vaccinated animals and infected patients. *J. Clin. Microbiol.* **58**, e01533-20.
- Walls, A.C., Fiala, B., Schafer, A., Wrenn, S., Pham, M.N., Murphy, M., Tse, L.V., Shehata, L., O'connor, M.A., Chen, C., et al. (2020). Elicitation of potent neutralizing antibody responses by designed protein nanoparticle vaccines for SARS-CoV-2. *Cell* **183**, 1367–1382 e17.
- Wang, L., Shi, W., Joyce, M.G., Modjarrad, K., Zhang, Y., Leung, K., Lees, C.R., Zhou, T., Yassine, H.M., Kanekiyo, M., et al. (2015). Evaluation of candidate vaccine approaches for MERS-CoV. *Nat. Commun.* **6**, 7712.
- Wanzeck, K., Boyd, K.L., and Mccullers, J.A. (2011). Glycan shielding of the influenza virus hemagglutinin contributes to immunopathology in mice. *Am. J. Respir. Crit. Care Med.* **183**, 767–773.
- Watanabe, Y., Allen, J.D., Wrapp, D., MCLELLAN, J.S., and CRISPIN, M. (2020). Site-specific glycan analysis of the SARS-CoV-2 spike. *Science* **369**, 330–333.
- Watanabe, Y., Bowden, T.A., Wilson, I.A., and Crispin, M. (2019). Exploitation of glycosylation in enveloped virus pathobiology. *Biochim. Biophys. Acta Gen. Subj.* **1863**, 1480–1497.
- Wei, X., Decker, J.M., Wang, S., Hui, H., Kappes, J.C., Wu, X., Salazar-Gonzalez, J.F., Salazar, M.G., Kilby, J.M., Saag, M.S., et al. (2003). Antibody neutralization and escape by HIV-1. *Nature* **422**, 307–312.
- Wu, F.W.A., Liu, M., Wang, Q., Chen, J., Xia, S., Ling, Y., Zhang, Y., Xun, J., Lu, L., et al. (2020). Neutralizing antibody responses to SARS-CoV-2 in a COVID-19 recovered patient cohort and their implications. *medRxiv*, 1–20.
- Wu, N.C., Yuan, M., Liu, H., Lee, C.D., Zhu, X., Bangaru, S., Torres, J.L., Caniels, T.G., Brouwer, P.J.M., Van Gils, M.J., et al. (2020a). An alternative binding mode of IGHV3-53 antibodies to the SARS-CoV-2 receptor binding domain. *Cell Rep.* **33**, 108274.
- Wu, Y., Wang, F., Shen, C., Peng, W., Li, D., Zhao, C., Li, Z., Li, S., Bi, Y., Yang, Y., et al. (2020b). A noncompeting pair of human neutralizing antibodies block COVID-19 virus binding to its receptor ACE2. *Science* **368**, 1274–1278.
- Xu, Z., Chokkalingam, N., Tello-Ruiz, E., Walker, S., Kulj, D.W., and Weiner, D.B. (2020a). Incorporation of a novel CD4+ helper epitope identified from Aquifex aeolicus enhances humoral responses induced by DNA and protein vaccinations. *iScience* **23**, 101399.
- Xu, Z., Chokkalingam, N., Tello-Ruiz, E., Wise, M.C., Bah, M.A., Walker, S., Tursi, N.J., Fisher, P.D., Schultheis, K., Broderick, K.E., et al. (2020b). A DNA-launched nanoparticle vaccine elicits CD8(+) T-cell immunity to promote in vivo tumor control. *Cancer Immunol. Res.* **8**, 1354–1364.
- Xu, Z., Wise, M.C., Chokkalingam, N., Walker, S., Tello-Ruiz, E., Elliott, S.T.C., Perales-Puchalt, A., Xiao, P., Zhu, X., Pumroy, R.A., et al. (2020c). In vivo assembly of nanoparticles achieved through Synergy of structure-based protein engineering and synthetic DNA generates enhanced adaptive immunity. *Adv. Sci.* **7**, 1902802.
- Yassine, H.M., Boyington, J.C., Mctamney, P.M., Wei, C.J., Kanekiyo, M., Kong, W.P., Gallagher, J.R., Wang, L., Zhang, Y., Joyce, M.G., et al. (2015). Hemagglutinin-stem nanoparticles generate heterosubtypic influenza protection. *Nat. Med.* **21**, 1065–1070.

- Yazici, M.K., Koc, M.M., Cetin, N.S., Karaaslan, E., Okay, G., Durdu, B., Sumbul, B., and Doymaz, M.Z. (2020). Discordance between serum neutralizing antibody titers and the recovery from COVID-19. *J. Immunol.* *205*, 2719–2725.
- Yu, J., Tostanoski, L.H., Peter, L., Mercado, N.B., McMahan, K., Mahrokhan, S.H., Nkolola, J.P., Liu, J., Li, Z., Chandrashekar, A., et al. (2020). DNA vaccine protection against SARS-CoV-2 in rhesus macaques. *Science* *369*, 806–811.
- Yuan, M., Liu, H., Wu, N.C., and Wilson, I.A. (2020a). Recognition of the SARS-CoV-2 receptor binding domain by neutralizing antibodies. *Biochem. Biophys. Res. Commun.* *538*, 192–203.
- Yuan, M., Wu, N.C., Zhu, X., Lee, C.D., So, R.T.Y., Lv, H., Mok, C.K.P., and Wilson, I.A. (2020b). A highly conserved cryptic epitope in the receptor binding domains of SARS-CoV-2 and SARS-CoV. *Science* *368*, 630–633.
- Zhang, B., Chao, C.W., Tsybovsky, Y., Abiona, O.M., Hutchinson, G.B., Molliva, J.I., Ollia, A.S., Pegu, A., Phung, E., Stewart-Jones, G.B.E., et al. (2020). A platform incorporating trimeric antigens into self-assembling nanoparticles reveals SARS-CoV-2-spike nanoparticles to elicit substantially higher neutralizing responses than spike alone. *Sci. Rep.* *10*, 18149.
- Zhao, L., Seth, A., Wibowo, N., Zhao, C.X., Mitter, N., Yu, C., and Middelberg, A.P. (2014). Nanoparticle vaccines. *Vaccine* *32*, 327–337.
- Zhou, D., Duyvesteyn, H.M.E., Chen, C.P., Huang, C.G., Chen, T.H., Shih, S.R., Lin, Y.C., Cheng, C.Y., Cheng, S.H., Huang, Y.C., et al. (2020a). Structural basis for the neutralization of SARS-CoV-2 by an antibody from a convalescent patient. *Nat. Struct. Mol. Biol.* *27*, 950–958.
- Zhou, P., Yang, X.L., Wang, X.G., Hu, B., Zhang, L., Zhang, W., Si, H.R., Zhu, Y., Li, B., Huang, C.L., et al. (2020b). A pneumonia outbreak associated with a new coronavirus of probable bat origin. *Nature* *579*, 270–273.

STAR★METHODS

KEY RESOURCES TABLE

REAGENT or RESOURCE	SOURCE	IDENTIFIER
<b>Antibodies</b>		
REGN10933	<a href="#">Hansen et al., 2020</a>	N/A
CV30	<a href="#">Seydoux et al., 2020</a>	N/A
CB6	<a href="#">Shi et al., 2020</a>	N/A
CC12.1	<a href="#">Rogers et al. 2020</a>	N/A
CC12.3	<a href="#">Rogers et al. 2020</a>	N/A
C144	<a href="#">Robbani et al., 2020</a>	N/A
C121	<a href="#">Robbani et al., 2020</a>	N/A
P2B-2F6	<a href="#">Ju et al., 2020</a>	N/A
C135	<a href="#">Robbani et al., 2020</a>	N/A
REGN10987	<a href="#">Hansen et al., 2020</a>	N/A
H4	<a href="#">Wu et al., 2020</a>	N/A
S309	<a href="#">Pinto et al., 2020</a>	N/A
EY6A	<a href="#">Zhou et al., 2020a</a>	N/A
COVD21_A11	<a href="#">Robbani et al., 2020</a>	N/A
CR3022	<a href="#">Yuan et al., 2020a</a>	N/A
CV43	<a href="#">Seydoux et al., 2020</a>	N/A
COVA2-44	<a href="#">Brouwer et al., 2020</a>	N/A
COVA2-45	<a href="#">Brouwer et al., 2020</a>	N/A
COVA2-46	<a href="#">Brouwer et al., 2020</a>	N/A
COVA3-06	<a href="#">Brouwer et al., 2020</a>	N/A
COVA2-24	<a href="#">Brouwer et al., 2020</a>	N/A
COVA1-08	<a href="#">Brouwer et al., 2020</a>	N/A
MonoRab anti-his tag C-term	Genscript	25B6E11
IR Dye 800CW goat anti-rabbit IgG	LI-COR Biosciences	926-32211
6x-His tag polyclonal antibody	Life Technologies	PA1983B
Goat anti-human IgG-Fc fragment	Bethyl Laboratories	A80-304P
Goat anti-mouse IgG h+i HRP-tagged antibody	Bethyl Laboratories	A90-116P
Peroxidase AffiniPure Goat Anti-Rat IgG	Jackson ImmunoResearch	112-035-071
Peroxidase AffiniPure F(ab') <sub>2</sub> Fragment Goat Anti-Rat IgM, $\mu$ chain specific	Jackson ImmunoResearch	112-036-075
Goat anti-Human Kappa Light Chain Antibody HRP Conjugated	Bethyl Laboratories	A80-115P
Goat anti-Human Lambda Light Chain Antibody HRP Conjugated	Bethyl Laboratories	A80-116P
Goat anti-Mouse IgG-heavy and light chain Antibody HRP Conjugated	Bethyl Laboratories	A90-116P
Goat anti-guinea pig IgG whole molecule	Sigma	A7289
Anti-Hamster IgG (H+L) Highly X-Adsorbed-HRP	Sigma	SAB3700451
anti-mouse CD107a-FITC antibody	BioLegend	121606
Live/Dead violet	Invitrogen	65-0863-14
CD4-BV510	BioLegend	100559
CD8-APC-Cy7	BioLegend	100714

(Continued on next page)

REAGENT or RESOURCE	SOURCE	IDENTIFIER
CD44-A700	BioLegend	103026
CD62L-BV711	BioLegend	104445
CD3e-PE-Cy5	BioLegend	100274
IFN- $\gamma$ -APC	BioLegend	505810
TNF- $\alpha$ -BV605	BioLegend	506329
<b>Bacterial and virus strains</b>		
SARS-CoV2 live virus (Washington strain)	BEI Resources	USA-WA1/2020, NR-52281
<b>Chemicals, peptides, and recombinant proteins</b>		
SARS-CoV-2 receptor binding domain peptides	Genscript	N/A
Recombinant RBD	Sino Biological	40592-V08
Recombinant RBD (K417T, E484K, N501Y)	Sino Biological	40592-V08H86
Recombinant RBD (N501Y)	Sino Biological	40592-V08H82
Recombinant RBD (K417N, E484K, N501Y)	Sino Biological	40592-V08H85
Recombinant RBD (L452R, E484Q)	Sino Biological	40592-V08H88
Human ACE2	In house	N/A
Intercept T20 (PBS) Antibody Diluent	LI-COR	927-75001
Intercept (PBS) Blocking Buffer	LI-COR	927-70001
1-Step™ Ultra TMB-ELISA Substrate Solution	Thermo Scientific	34029
RIBI adjuvant	Sigma Aldrich	S6322-1VL
SARS-CoV-2 RBD (amino acids 331-527)	In house	N/A
Cell stimulation cocktails plus protein transport inhibitors	Invitrogen	00-4975-93
Protein Transport Inhibitor Cocktail	Invitrogen	00-4980-93
Cell Stimulation Cocktail	Invitrogen	00-4970-93
SureBlue TMB 1-Component Microwell Peroxidase Substrate	KPL	5120-0075
TMB Stop Solution	KPL	5150-0020
Trypsin (Mass Spectrometry Grade)	Promega	90058
Chymotrypsin (Mass Spectrometry Grade)	Promega	90056
Alpha-lytic protease	Sigma Aldrich	A6362
<b>Critical commercial assays</b>		
BriteLite plus luminescence reporter system	Perkin Elmer	6066769
Mouse IFN- $\gamma$ ELISpotPLUS plates	MabTech	3321-4APT-10
96-well flat bottom, half-area plates	Corning	3690
<b>Experimental models: Cell lines</b>		
293T	ATCC	CRL-3216
Vero	ATCC	CCL-81
CHO cells expressing human ACE2 receptors	Creative Biolabs	VCel-Wyb030
<b>Experimental models: Organisms/strains</b>		
Mouse C57BL/6	Jackson Laboratories	N/A
Mouse BALB/c	Jackson Laboratories	N/A
Mouse Omni Mouse®	Ligand Pharmaceuticals Incorporated	N/A
Mouse K18-hACE2	Jackson Laboratories	N/A
Hartley guinea pig	Elm Hill Labs	N/A

(Continued on next page)

**Continued**

REAGENT or RESOURCE	SOURCE	IDENTIFIER
Golden Syrian hamster	Envigo	N/A
<b>Recombinant DNA</b>		
RBD g3.1	This study	N/A
RBD g3.2	This study	N/A
RBD g3.3	This study	N/A
RBD g5.1	This study	N/A
RBD g8.1	This study	N/A
RBD g8.2	This study	N/A
RBD g8.3	This study	N/A
RBD 48mer	This study	N/A
RBD g5.1 7mer	This study	N/A
RBD g5.1 14mer	This study	N/A
RBD g5.1 60mer	This study	N/A
RBD g5.1 120mer	This study	N/A
RBD g5.1 180mer	This study	N/A
RBD g8.1 7mer	This study	N/A
RBD g8.1 60mer	This study	N/A
RBD g8.1 120mer	This study	N/A
RBD g8.1 180mer	This study	N/A
RBD g8.2 7mer	This study	N/A
RBD g8.2 60mer	This study	N/A
RBD g8.2 120mer	This study	N/A
RBD g8.2 180mer	This study	N/A
RBD g8.3 7mer	This study	N/A
RBD g8.3 60mer	This study	N/A
RBD g8.3 120mer	This study	N/A
RBD g8.3 180mer	This study	N/A
P.1 RBD g5.1 24mer	This study	N/A
S_IgE_deltaCterm19 plasmid	Genscript	N/A
S_SA_IgE_deltaCterm19 plasmid	Genscript	N/A
S_UK_IgE_deltaCterm19 plasmid	Genscript	N/A
S_Brazil_IgE_deltaCterm19 plasmid	Genscript	N/A
pNL4-3.luc.R-E- backbone	Aldevron	N/A
<b>Software and algorithms</b>		
GraphPad Prism (version 8 or later)	GraphPad	N/A
Pymol (version 2.4 or later)	Schrodinger	N/A
Biorender	Biorender	N/A
Biacore Insight Evaluation	Cytiva	N/A
Flowjo (version 10)	BD Biosciences	N/A
Molecular Software Libraries (version 1.3 alpha)	<a href="http://msl-libraries.org/">http://msl-libraries.org/</a>	N/A
Rosetta software suite (v201.42.02-59804)	Rosetta Commons	N/A
R (version 1.4.1103)	R Core Team	N/A
Relion (version 3.1.2)	MRC Laboratory of Molecular Biology	N/A
Byonic™ (version 4.0)	Protein Metrics Inc.	N/A
CWG	<a href="https://doi.org/10.5281/zenodo.5762081">https://doi.org/10.5281/zenodo.5762081</a>	5762081

(Continued on next page)

REAGENT or RESOURCE	SOURCE	IDENTIFIER
<b>Continued</b>		
Other		
AKTA Pure 25 purification system	GE	N/A
HisTrap™ HP prepacked Column	Cytiva	45000325
Agarose bound Galnthus Nivalis Lectin beads	Vector Labs	AL-1243-5
Superdex 200 Increase 10/300 GL column	GE	28990944
Superose 6 Increases 10/300 GL column	GE	29091596
HiTrap™ MabSelect™ SuRe Protein A column	Cytiva	45000009
Odyssey CLx	LI-COR	N/A
Synergy 2 plate reader	BioTek	N/A
Synergy HTX plate reader	BioTek	N/A
Biacore 8 k instrument	GE	N/A
Series S Sensor Protein A capture chip	Cytiva	501055504
Tecnai T12 microscope	FEI	N/A
Oneview	Gatan	N/A
Vitrobot Mark IV robot	FEI	N/A
Talos Arctica electron microscope	FEI	N/A
Falcon 3 camera	FEI	N/A
CTL reader	ImmunoSpot	N/A
18-color LSRII flow cytometer	BD Biosciences	N/A
LC-ESI MS with an Ultimate 3000 HPLC	Thermo Fisher Scientific	N/A
Orbitrap Eclipse mass spectrometer	Thermo Fisher Scientific	N/A
PepMap 100 C18 column 3 μM 75 μm x 2cm	Thermo Scientific	164535

## RESOURCE AVAILABILITY

### Lead contact

Further information and requests for resources and reagents should be directed to and will be fulfilled by the lead contact, Daniel W. Kulp ([dwkulp@wistar.org](mailto:dwkulp@wistar.org)).

### Materials availability

Unique reagents (i.e. plasmids, pseudoviruses) generated in this study will be made available on request, but we may require payment and/or completed Materials Transfer Agreement if there is potential for commercial application.

### Data and code availability

Data pertaining to these studies will be made available upon request. Additional Supplemental Items are available from Mendeley Data: <https://doi.org/10.17632/nvnkv277mg.1>. Glycan modeling code generated in these studies is available at Zendo: <https://doi.org/10.5281/zenodo.5762081> and Rosetta is available at GitHub: <https://github.com/RosettaCommons>. Any additional information required to reanalyze the data reported in this paper is available from the lead contact on upon request.

## EXPERIMENTAL MODEL AND SUBJECT DETAILS

### Animals

BALB/c and C57BL/6 mice (female, 6–8 weeks old) were utilized in these studies to assess antibody responses after immunization and cellular responses. Mice were given free access to food and water and housed in the Wistar animal facility in ventilated cages in accordance with Wistar Institutional Animal Care and Use Committees under approved animal protocols.

Omni Mouse® (female, 12–18 weeks old) for human antibody studies were obtained from Ligand Pharmaceutical Incorporated. Mice were given free access to food and water and housed in the Wistar animal facility in ventilated cages in accordance with Wistar Institutional Animal Care and Use Committees under approved animal protocols.

K18-hACE2 transgenic mice (male and female, 6–8 weeks old) were utilized for the model of SARS-CoV2 lethal challenge. Mice were given free access to food and water and housed in the Wistar animal facility in ventilated cages in accordance with Wistar Institutional Animal Care and Use Committees under approved animal protocols. For lethal challenge, mice were shipped to Texas Biomed and blinded to treatment groups. A weight loss cutoff of 20% was used as euthanasia criterion.

Hartley guinea pigs and golden Syrian hamsters (female, 8 weeks old) were housed at Acculab Life Sciences animal facilities and treated under approved animal protocols from Acculab Institutional Animal Care and Use Committees.

### Cell lines

CHO and 293T cells (passage 8–16) were used for pseudovirus generation and neutralization studies. Vero cells were used for live virus neutralization studies.

## METHOD DETAILS

### Cloaking with glycans algorithm

The modeling started with RBD structure PDB id: 6M0J. GlycanTreeModeler(GTM) is a glycan modeling algorithm recently developed in Rosetta(unpublished). The Cloaking With Glycans (CWG) workflow utilizes GTM for selecting single glycan addition positions on target protein. All steps in CWG are summarized in a flowchart (Figure 1B). CWG begins with detecting native sequons and modeling all the native glycan structures using Man9GlcNAc2 glycans on the target protein. In the next stage, a model is made for the addition of a single glycan at each position. A given position in the protein is mutated to asparagine and the i+2 position is mutated into threonine or serine. The model with the lowest energy i+2 position is used for further evaluation. The Rosetta energy is computed for the resulting model. We filtered out positions if the total energy of the model corresponding to that position had a total energy >5 Rosetta Energy Units (REU) more than the native structure. Next, the CWG algorithm builds Man9GlcNAc2 glycans on the mutated position and measures repulsive energy of engineered glycan between sugar-sugar and sugar-protein energy terms. We filtered out some positions based on structural criteria, such as avoiding the mutation of positions involved in disulfide bonds. Man9GlcNAc2 glycans were utilized for simplicity.

### Nanoparticle modeling

All nanoparticles were modeled with corresponding designed structures and linkers. Four nanoparticles were used in this study: IMX313P (PDB id: 4B0F), ferritin (PDB id: 3BVE), lumazine synthase (PDB id: 1HQK), and PcV (PDB id: 3J3I). Biological unit nanoparticle structure files were downloaded in CIF format. The termini of the monomeric RBDs were aligned to the termini of the nanoparticle, rotational and translational degrees of freedom were sampled to reduce clashing between RBDs and nanoparticles, extended linkers of various lengths were then aligned to fuse the nanoparticle and immunogen with simpleNanoparticleModeling from the MSL library as previously described (Xu et al., 2020c).

### Protein expression and purification

Glycosylated RBDs: A gene encoding the amino acids 331–527 of the SARS-CoV-2 spike glycoprotein (PDB: 6M0J) was mutated at each position according to CWG. Nanoparticles were genetically fused to designed RBDs as described above. DNA encoding the variants were codon optimized for homo sapiens and cloned with a IgE secretion sequence into the pVAX vector. A 6xHisTag was added to the c-terminus of the RBD monomer variants. ExpiF293 cells were transfected with the pVAX plasmid vector either carrying the nanoparticles or the His-Tagged monomer transgene with PEI/Opti-MEM and harvested 6–7 days post transfection. The supernatants was first purified with affinity chromatography using the AKTA pure 25 purification system and IMAC Nickel column (HisTrap™ HP prepacked Column, Cytiva) for His-tagged monomers and gravity flow columns filled with Agarose bound Galnthus Nivalis Lectin beads (Vector Labs) for nanoparticles. The eluate fractions from the affinity chromatography were pooled, concentrated, and dialyzed into 1X PBS before being loaded onto the Size-Exclusion Chromatography (SEC) column for further purification with Superdex 200 Increase 10/300 GL column for the His-tagged monomers and the Superose 6 Increases 10/300 GL column for the nanoparticles. Fractions of interest were pooled and concentrated for characterization. For antibody production, heavy and light chains were encoded in pFUSEss-CHlg-hG1, and pFUSE2ss-CLlg-hk or pFUSEss-CLlg-hL2 respectively and were co-transfected in equal parts using ExpiFectamine™ 293 Transfection Kit(Gibco) according to manufacturer's protocol. Antibodies were purified by affinity chromatography using the Protein A column (HiTrap™ MabSelect™ SuRe, Cytiva) and AKTA Pure 25 purification system.

### Western Blot

Samples were prepared with 13  $\mu$ L supernatants of Expi293F cells transfected with RBD monomer plasmids or 0.65  $\mu$ g of purified WT RBD in 1x PBS, NuPAGE LDS Sample Buffer (Novex), and NuPAGE Sample Reducing Agent (Novex) were denatured at 90°C for 10 minutes. Samples were loaded in a 4–12% SDS Bis-Tris gel for electrophoresis then transferred from the gel onto a PVDF membrane. The membrane was blocked with Intercept (PBS) Blocking Buffer (LI-COR) for >1 h at ambient temperature then incubated with 1.25  $\mu$ g/protein gel of MonoRab anti-his tag C-term (Genscript) in Intercept T20 (PBS) Antibody Diluent (LI-COR) overnight at 4°C. The membrane was then incubated in a 1:10000 IRDye 800CW goat anti-rabbit IgG (LI-COR Biosciences) in Intercept T20 (PBS) Antibody Diluent (LI-COR) at room temperature for 1 h. Membranes were imaged with a LI-COR Odyssey CLx.

### ELISA

For *in vitro* characterization, high Binding, 96-well Flat-Bottom, Half-Area Microplate (Corning) were coated at 1  $\mu\text{g}/\text{mL}$  6x-His tag polyclonal antibody (Invitrogen) for >4 hours at ambient temperature and blocked  $\geq 1$  hour with 5% milk/1x PBS/0.01% Tween-20 at 4°C. RBD transfection supernatant or recombinant protein at 10  $\mu\text{g}/\text{mL}$  was incubated for 1-2 hours at ambient temperature. Serial dilutions of antibodies were made according to affinity and incubated on plate for 1-2 hours at ambient temperature. Goat anti-Human IgG-Fc fragment cross-adsorbed antibody HRP conjugated (Bethyl Laboratories) secondary at a 1:10,000 dilution for 1 hour at ambient temperature. All dilutions except coating were performed in 5% milk/1x PBS/0.01% Tween-20 and plates were washed with 1x PBS/0.05% Tween-20 between steps. 1-Step™ Ultra TMB-ELISA Substrate Solution (Thermo Scientific) was incubated on the plate for 10 minutes in the dark and then quenched with 1 M  $\text{H}_2\text{SO}_4$ . Absorbance of samples at 570 nm was subtracted from 450 nm for each well and background of blank wells were subtracted from each well before analysis. Curves were analyzed in GraphPad Prism 8 with Sigmoidal, 4PL, X is concentration and AUC.

For serology, plates were coated with 1  $\mu\text{g}/\text{mL}$  6x-His tag polyclonal antibody (Invitrogen) in 1x PBS for 6 hours at ambient temperature and blocked overnight with 0.5% NCS/5% Goat Serum/5% Milk/0.2% PBS-T. 5x serial dilutions of sera were made starting at a 1:100 dilution and incubated on plate for 2 hours at 37°C. For BL6, BALB/c, and K18 ACE2 mouse studies, goat anti-mouse IgG h-I HRP-tagged antibody (Bethyl Laboratories) diluted 1:20000. For the OmniMouse® study, Peroxidase AffiniPure Goat Anti-Rat IgG (Jackson ImmunoResearch) at 1:10000, Peroxidase AffiniPure F(ab)<sub>2</sub> Fragment Goat Anti-Rat IgM,  $\mu$  chain specific (Jackson ImmunoResearch) at 1:10000, Goat anti-Human Kappa Light Chain Antibody HRP Conjugated (Bethyl Laboratories) at 1:10000, Goat anti-Human Lambda Light Chain Antibody HRP Conjugated (Bethyl Laboratories) at 1:10000, and Goat anti-Mouse IgG-heavy and light chain Antibody HRP Conjugated (Bethyl Laboratories) at 1:20000, and Goat anti-guinea pig IgG whole molecule (Sigma) at 1:10,000 were used. Secondary antibodies were incubated on plates for 1 hr at RT. All dilutions except coating were performed in 1% NCS in 0.2% PBS-T and plates were washed with 1x PBS/0.05% Tween-20 between steps. Plates were developed with 1 Step Ultra TMB substrate in the dark for 10 minutes for mouse studies and 15 minutes for guinea pig studies before being quenched with 1N  $\text{H}_2\text{SO}_4$  and read using a BioTek Synergy 2 plate reader at an absorbance of 450 and 570 nm.

Hamster serology was performed by directly coating 96-well flat bottom, half-area plates #3690 (Corning) with 25  $\mu\text{L}$  of 1  $\mu\text{g}/\text{mL}$  of SARS-CoV-2 RBD (University of Texas, Austin) overnight at 4°C. Plates were blocked with 100  $\mu\text{L}$  of blocking buffer (3% BSA in 1x PBS) for 1 h at 37°C. Hamster sera was diluted to 1:16 dilution in diluent buffer (1% BSA in PBS) and an 11-point 1:3 serial dilution was done on the ELISA plate, with last column containing only dilution buffer as blank control. ELISA plates were incubated for 2 h at 37°C with sera dilutions. Anti-Hamster HRP antibody (Sigma) was diluted in diluent buffer 1:10,000 and were incubated for 1 hr at room temperature. SureBlue TMB 1-Component Microwell Peroxidase Substrate (KPL) was added to the wells and plates were incubated for 6 minutes and then quenched with TMB Stop Solution (KPL). Absorbance was immediately read at 450 nm on Synergy HTX plate reader (BioTek). All volumes except blocking buffer was 25  $\mu\text{L}$ . Plates were washed 3 times with wash buffer (.05% Tween 20 in 1x PBS) between steps.

### Surface plasmon resonance

RBD-antibody kinetics experiments were performed with a Series S Sensor Protein A capture chip (Cytiva) on a Biacore 8 k instrument (GE). The running buffer was HBS-EP (3 M sodium chloride/200 mM HEPES/60 mM EDTA/1.0% Tween 20 pH=7.6) (Teknova) with 0.1% (w/v) bovine serum albumin. Each experiment began with two start up cycles with 60 s of contact time and a flow rate of 50  $\mu\text{L}/\text{min}$ . For analysis methods, approximately 200-300 RUs of IgG antibodies was captured on each flow cell at a flow rate of 10  $\mu\text{L}/\text{min}$  for 60 seconds. WT RBD or glycan variants samples were 5x serial diluted from 1000 nM in running buffer and flowed across the chip after capture at a 50  $\mu\text{L}/\text{min}$  rate. The experiment had a 120 second contact time phase and 600 seconds dissociation phase. Regeneration was performed with 10 mM glycine at pH=1.5 at a flow rate of 50  $\mu\text{L}/\text{min}$  for 30 seconds after each cycle. Kinetic fits were analyzed with 1:1 fitting and run through a script to filter out results that had poor fitting, low max RUs compared to expected, and *k<sub>on</sub>* and *k<sub>off</sub>* constants that fell outside of the range of measurement. Experiments that were flagged as poor-quality fitting by this script were not further analyzed.

### Pseudovirus neutralization assay

HEK293T (CRL-3216) were obtained from ATCC (Manassas, VA, USA). Cells were maintained in DMEM supplemented with 10% fetal bovine serum (FBS) and 1% penicillin-streptomycin (P/S) antibiotic at 37°C under 5%  $\text{CO}_2$  atmosphere. For luciferase-based virus pseudoneutralization assays, HEK293T cells were transfected to produce SARS-CoV-2 S containing pseudoviruses. Cells were seeded at 5 million cells onto T75 flasks and grown for 24 hours. Then, cells were treated with 48  $\mu\text{L}$  GeneJammer (Agilent 204130-21), 6  $\mu\text{g}$  S\_IgE\_deltaCterm19\_plasmid (Genscript), and 6  $\mu\text{g}$  pNL4-3.luc.R-E- backbone (Aldevron) and incubated for 48 hours. For variant pseudoviruses, cells were similarly treated with GeneJammer and backbone with 6  $\mu\text{g}$  of S\_SA\_IgE\_deltaCterm19, S\_UK\_IgE\_deltaCterm19, or S\_Brazil\_IgE\_deltaCterm19 plasmid. Transfection supernatants were then collected and supplemented with 12% FBS, sterile filtered, and stored at  $-80^\circ\text{C}$ . Pseudovirus solutions were titered and dilution to working solutions set such that they yielded >215-fold greater relative luminescence units (RLS) than cells alone.

CHO cells expressing human ACE2 receptors (VCel-Wyb030) were obtained from Creative Biolabs (Shirley, NY). CHO-ACE2 cells were seeded at 10,000 cells/well in 96-well plates and incubated for 24 hours. Sera from vaccinated mice were heat inactivated at 56°C for 15 minutes. 3-fold serial dilutions starting at 1:20 dilutions in DMEM supplemented with 10% FBS and 1% P/S were

performed on sample sera and incubated for 90 minutes at room temperature with SARS-CoV2 pseudovirus based on concentrations determined from titering described above. Media containing diluted sera and pseudovirus were then applied to CHO-ACE2 cells. After 72 hours of incubation, cells were developed using Britelite plus luminescence reporter system (Perkin Elmer 6066769) and signal measured using a plate reader (Biotek Synergy). Percent neutralization was calculated based on virus only positive control signal with background subtraction of cells only negative controls. ID<sub>50</sub> values were calculated using GraphPad Prism v8.0 nonlinear curve fitting with constraint Hill Slope <0.

### SARS-CoV-2 culture, titer, and neutralization assay

SARS-Related Coronavirus 2, Isolate USA-WA1/2020, NR-52281 was deposited by the Centers for Disease Control and Prevention and obtained through BEI Resources, NIAID, NIH. All work with it was performed in the BSL-3 facility at the Wistar Institute. Vero cells (ATCC CCL-81) were maintained in antibiotic-free Dulbecco's modified Eagle's medium (DMEM) supplemented with 10% fetal bovine serum (FBS). To grow a stock of virus, 3 million Vero cells were seeded in a T-75 flask for overnight incubation (37°C, 5% CO<sub>2</sub>). The cells were inoculated the next day with 0.01 MOI virus in DMEM. Culture supernatant was harvested 3 days post infection, aliquoted, and stored at -80°C. For titering the virus stock, Vero cells were seeded in DMEM with 1% FBS at 20,000 cells/well in 96 well flat bottom plates for overnight incubation (37°C, 5% CO<sub>2</sub>). The USA-WA1/2020 virus stock was serially diluted in DMEM with 1% FBS and transferred in replicates of 8 to the previously seeded Vero cells. Five days post infection individual wells were scored positive or negative for the presence of cytopathic effect (CPE) by examination under a light microscope. The virus titer (TCID<sub>50</sub>/ml) was calculated using the Reed-Munch method and the Microsoft Excel based calculator published by Lei et al. (Lei et al., 2021) For neutralization assays, Vero cells were seeded in DMEM with 1% FBS at 20,000 cells/well in 96 well flat bottom plates for overnight incubation (37°C, 5% CO<sub>2</sub>). Serum samples were heat inactivated at 56°C for 30 minutes. Serum samples were then serially diluted in DMEM with 1% FBS and 1% penicillin/streptomycin and incubated for one hour at room temperature with 300 TCID<sub>50</sub>/ml USA-WA1/2020. The serum-virus mixture was then transferred in triplicate to the previously seeded Vero cells. Five days post infection, individual wells were scored positive or negative for the presence of CPE and neutralization titers were calculated using the Reed-Munch method and a modified version of the Microsoft Excel based calculator published by Lei et al. (Lei et al., 2021).

### Animal studies

C57BL/6, BALBc, and K18-hACE2 mice were obtained from Charles River Laboratories (Malvern, PA) and The Jackson Laboratory (Bar Harbor, ME). Omni Mouse® for human antibody studies were obtained from Ligand Pharmaceuticals Incorporated (San Diego, CA). All studies were performed in accordance with Wistar Institutional Animal Care and Use Committees under approved animal protocols. All animals were housed in the Wistar animal facility in ventilated cages and given free access to food and water. For the lethal challenge study, Texas Biomed were blinded to identity of vaccination groups and weight loss cutoff for euthanasia was 20%. For protein immunizations, mice were administered subcutaneously in 100µL PBS co-formulated with RIBI adjuvant (Sigma Aldrich). For DNA immunizations, intramuscular injection with electroporation and sample collection. Plasmids were administered intramuscularly in 30µL water into the tibialis anterior muscle. Electroporation was then performed using CELLECTRA EP delivery platform consisting of two pulse sets at 0.2 Amps at a 3 second interval. Each pulse set consists of two 52 ms pulses with 198 ms delay. At specified time points, blood was collected via submandibular vein puncture and centrifuged for 10 min at 15000 rpm to obtain sera. For cellular responses, mice were euthanized under CO<sub>2</sub> overdose. Spleens were collected into cold RPMI media supplemented with 10% FBS and 1% P/S.

Female Hartley guinea pigs (8 weeks old, Elm Hill Labs, Chelmsford MA) were housed at Acculab (San Diego CA). On day 0 and day 28 animals were anaesthetized with isoflurane vapor and received intradermal Mantoux injections of 100 µL 10, 5 or 0.5 µg pDNA immediately followed by CELLECTRA-3P electroporation. The CELLECTRA® EP delivery consists of two sets of pulses with 0.2 Amp constant current. Second pulse set is delayed 3 seconds. Within each set there are two 52 ms pulses with a 198 ms delay between the pulses. Serum samples were collected by jugular or saphenous blood collection throughout the study on days 0, 7, 14, 21, 28 and 42. Whole blood samples to process PBMCs for cellular assay were collected from the jugular vein on days 14 and 42. All animals were housed in the animal facility at Acculab Life Sciences (San Diego, CA). All animal protocols were approved by Acculab Institutional Animal Care and Use Committees (IACUC).

Golden Syrian hamsters (8 weeks old, Envigo, Indianapolis, IN) were housed at Acculab (San Diego, CA). Hamsters received intramuscular (IM) injections of 60 µL of 2 or 10 µg pDNA formulation into the tibialis anterior muscle immediately followed by electroporation with the CELLECTRA-3P device under isoflurane vapor anesthesia at day 0 and day 21. The CELLECTRA® EP delivery consists of two sets of pulses with 0.2 Amp constant current. Second pulse set is delayed 4 s. Within each set there are two 52 ms pulses with a 198 ms delay between the pulses. Serum samples were collected at indicated timepoints via saphenous vein blood collection throughout the experiment. All animals were housed in the animal facility at Acculab Life Sciences (San Diego, CA). All animal protocols were approved by Acculab Institutional Animal Care and Use Committees.

In-vivo study was concluded with terminal blood, lung lavage and nasal wash collection. Lavage buffer was prepared as PBS containing 100µM EDTA, 0.05% Sodium Azide, 0.05% Tween-20 and Protease Inhibitor. Hamsters were euthanized by jugular exsanguination with intraperitoneal (IP) injection of 86.7 mg/kg pentobarbital sodium or overdose isoflurane gas inhalation. Euthanized hamster was placed in supine position and skin was disinfected using 70% Isopropyl alcohol. A longitudinal cut using scissors

and blunt dissection along the midline of the neck was performed to expose the trachea. An opening into the exposed trachea was created by making a transverse, semilunar cut using #11 blade.

To collect nasal wash an 18ga blunt end needle was inserted toward the nose and gently proceeded upwards until reaching the nasal palate. A syringe filled with 1.5 mL lavage buffer was connected to the blunt end needle and correct placement was tested by dispensing a small amount through the hamster's nares. The entire volume of lavage fluid was rapidly dispensed and collected directly from the nares into a 5.0 mL Eppendorf tube.

To collect bronchioalveolar lavage (BAL), an 18ga blunt end needle, attached to a three-way stopcock and primed with lavage buffer (approximately 0.5 mL) to eliminate empty airspace, was inserted forward until just prior to the tracheal bifurcation into the lungs. The blunt end needle was secured in the trachea with a silk 2-0 tie. A 3 mL receiver syringe and a 10 mL syringe filled with 9 mL of lavage buffer was connected to the blunt end needle via the three-way stopcock. The lungs were rinsed three times (3 mL each time) with a total of 9 mL lavage buffer. Typically, 50% of lavage buffer was recovered.

### Hamster biodistribution

Lung lavage and nasal wash samples were ultrafiltrated using a 2 mL 100 kDa cut-off ultrafiltration device (Millipore, Burlington MA) spinning 1 mL BAL or NW for 15 min at 4000 g. Ultrafiltrated BAL was diluted 1:6 and nasal wash was diluted 1:4 in ELISA dilution buffer and following washes and blocking as described in the ELISA section added to half area assay plates (Costar) coated with 25  $\mu$ L/well of 1  $\mu$ g/mL SARS-CoV-2 RBD (Sinobiological) in dilution buffer overnight at 4C. BAL and NW samples were tested at a 7-step 1:2 serial dilution.

### Negative-stain electron microscopy

Purified RBD g5.1 nanoparticle was dialyzed into 20 mM HEPES buffer, 0.15M NaCl, pH 7.4. A total of 3  $\mu$ L of purified proteins was adsorbed onto glow discharged carbon-coated Cu400 EM grids. The grids were then stained with 3  $\mu$ L of 2% uranyl acetate, blotted, and stained again with 3  $\mu$ L of the stain followed by a final blot. Image collection and data processing was performed on a FEI Tecnai T12 microscope equipped with Oneview Gatan camera at 90 450 $\times$  magnification at the camera and a pixel size of 1.66  $\text{\AA}$ .

### Cryo electron microscopy

Cryo-EM vitrification was obtained in a Vitrobot Mark IV robot (FEI). Four  $\mu$ L of purified RBD g5.1 24mer nanoparticles in 1xPBS were deposited on a glow-discharged holey carbon grid (C-flat 1.2/1.3, 300 mesh; Protochips). Excess liquid was blotted away followed by immediate plunging into liquid ethane cooled by liquid nitrogen. The vitrified specimen was then introduced into an FEI Talos Arctica electron microscope (FEI). Automated data collection was performed in EPU (FEI) and 640 movie micrographs were recorded with a Falcon 3 camera (FEI) at 150,000 $\times$  magnification corresponding to an image pixel size of 0.97  $\text{\AA}$  on the object scale. Each movie micrograph comprised 50 frames, each frame was exposed with a dose of  $\sim 1 e^-/\text{\AA}^2$ . Data processing was performed in Relion v3.1.2 (Scheres, 2012). Movie micrograph frame alignment, spectral signal weighing and summation was followed by CTF modeling (CTFFIND4 (Rohou and Grigorieff, 2015)). Candidate molecular projection images were identified with Relion LoG picking ( $\sim 271,000$ ). Image windows corresponding to the candidate molecular projection image coordinates were extracted and binned by a factor of 2. The extracted binned data was subjected to 2D classification. Manual inspection of class averages led to identification of 93,348 molecular projection images selected for further data processing. Molecular projections were re-extracted unbinned from the summed micrographs and iterative Euler angular reconstitution and 3D object reconstruction was performed with a low-resolution ferritin density map as initial seed. 3D refinement was performed both asymmetrically (FSC 0.143 resolution 3.98  $\text{\AA}$ ) and under the assumption of octahedral symmetry (FSC 0.143 resolution 3.42  $\text{\AA}$ ). Since our objective was to map the attachment sites of the RBDs to the ferritin cage, we made no efforts to improve ferritin particle alignment in our refinement strategy for the present manuscript.

### ELISpot assay

Spleens from immunized mice were processed by a tissue stomacher, and red blood cells were then lysed by ACK buffer (Thermo Fisher Scientific). Single cell suspension was counted, and  $2 \times 10^5$  splenocytes were plated into each well of the Mouse IFN- $\gamma$  ELISpotPLUS plates (MabTech). The splenocytes were stimulated for 20 hours at 37 $^\circ$ C with RBD peptides (15-mer peptides overlapping by 9 amino acid spanning the RBD of SARS-CoV-2 spike protein, GenScript), at 5  $\mu$ g/mL of each peptide in RPMI + 10% FBS (R10). The spots were developed according to manufacturer's instructions. R10 and cell stimulation cocktails (Invitrogen) were used for negative and positive controls, respectively. Spots were scanned and quantified by ImmunoSpot CTL reader. Spot-forming unit (SFU) per million cells was calculated by subtracting the negative control wells.

### Intracellular cytokine staining and flow cytometry

Splenocytes were processed as described in the previous section and stimulated with RBD peptides for 5 hours at 37 $^\circ$ C with protein transport inhibitor (Invitrogen) and anti-mouse CD107a-FITC antibody (BioLegend). Cell stimulation cocktail and R10, with protein transport inhibitor, were used as positive and negative controls, respectively. After stimulation, cells were stained with Live/Dead violet (Invitrogen) for viability. Anti-mouse CD4-BV510, CD8-APC-Cy7, CD44-A700, and CD62L-BV711 antibodies were used for

surface staining and CD3e-PE-Cy5, IFN- $\gamma$ -APC, and TNF- $\alpha$ -BV605 (all from BioLegend) were used for intracellular staining. The samples were run on an 18-color LSRII flow cytometer (BD Biosciences) and analyzed by FlowJo software.

### Competition assay

96-well Flat-Bottom Half-Area plates (Corning) were coated at room temperature for 8 hours with 1  $\mu$ g/mL 6x-His tag polyclonal antibody (PA1-983B, ThermoFisher), followed by overnight blocking with blocking buffer containing 5% milk/1x PBS/0.01% Tween-20 at 4°C. The plates were then incubated with RBD at 1  $\mu$ g/mL at room temperature for 1-2 hours. Mouse Sera (BALB/c, terminal bleeds, week 6, n=5) either immunized with RBD-WT or RBD-gPenta was serially diluted 3-fold starting at 1:20 with dilution buffer (5% milk/1x PBS/0.01% Tween-20) was added to the plate and incubated at room temperature for 1-2 hours. Plates were then washed and incubated at room temperature for 1 hour with ACE2-IgHu at a constant concentration of 0.06  $\mu$ g/mL diluted with the dilution buffer. After being washed, the plates were further incubated at room temperature for 1 hour with goat-anti human IgG-Fc fragment cross-adsorbed Ab (A80-340P; Bethyl Laboratories) at a 1: 10,000 dilution, followed by addition of TMB substrates (ThermoFisher), and then quenched with 1M H<sub>2</sub>SO<sub>4</sub>. Absorbances at 450 nm and 570 nm were recorded with a BioTek plate reader. Four washes were performed between every incubation step using PBS and 0.05% Tween-20. The assay was performed in triplicates. The average absorbance of the lowest dilutions with saturating ACE2 signals was calculated to get a maximum ACE2 binding and no blocking. Each average absorbance value was subtracted from the maximum to get an ACE2 blocking curve. The blocking titer is defined as the reciprocal of the highest dilution where two consecutive dilutions have readings below zero. The maximum area under the curve is determined by calculating the Area Under the Curve (AUC) of full ACE2 binding without the competitor. The AUC of the competitor is then subtracted from the maximum AUC which provides the area between the two curves (blocking area) and is a measure of ACE2 blocking. The fraction ACE2 blocking is defined as the fraction of the blocking area to the maximum AUC.

### Site-specific glycan analysis using mass spectrometry

RBD proteins were denatured for 1 h in 50 mM Tris/HCl, pH 8.0 containing 6M of urea and 5 mM dithiothreitol (DTT). Next, the proteins were reduced and alkylated by adding 20 mM iodacetamide (IAA) and incubated for 1 h in the dark, followed by a 1 h incubation with 20 mM DTT to eliminate residual IAA. The alkylated proteins were buffer-exchanged into 50 mM Tris/HCl, pH 8.0 using Vivaspin columns (3 kDa) and digested separately overnight using three protease enzymes in separate tubes, trypsin, (Mass Spectrometry Grade, Promega), Chymotrypsin (Mass Spectrometry Grade, Promega), Alpha-lytic protease (Sigma-Aldrich) at a ratio of 1:30 (w/w). The next day, the peptides were dried and extracted using C18 Zip-tip (MerckMilipore). The peptides were dried again, re-suspended in 0.1% formic acid and analyzed by nano LC-ESI MS with an Ultimate 3000 HPLC (Thermo Fisher Scientific) system coupled to an Orbitrap Eclipse mass spectrometer (Thermo Fisher Scientific) using stepped higher energy collision-induced dissociation (HCD) fragmentation. Peptides were separated using an EasySpray PepMap RSLC C18 column (75  $\mu$ m  $\times$  75 cm). A trapping column (PepMap 100 C18 column 3  $\mu$ M 75  $\mu$ m  $\times$  2 cm) was used inline prior to separation with the analytical column. The LC conditions were as follows: 280-minute linear gradient consisting of 4–32% acetonitrile in 0.1% formic acid over 260 minutes followed by 20 minutes of alternating 76% acetonitrile in 0.1% formic acid and 4% acetonitrile in 0.1% formic acid, used to ensure all the samples has eluted from the column. The flow rate was set to 200 nL/min. The spray voltage was set to 2.7 kV and the temperature of the heated capillary was set to 40°C. The ion transfer tube temperature was set to 275°C. The scan range was 375–1500 m/z. The stepped HCD collision energy was set to 15%, 25%, 45%, appropriate for fragmentation of glycopeptide ions. Precursor and fragment detection were performed using an Orbitrap at a resolution MS1 = 100,000. MS2 = 30,000. The AGC target for MS1 was set to standard and injection time set to auto which involves the system setting the two parameters to maximize sensitivity while maintaining cycle time. Full LC and MS methodology can be extracted from the appropriate raw file using XCalibur FreeStyle software.

Glycopeptide fragmentation data were extracted from the raw file using Byonic<sup>TM</sup> (Version 4.0; Protein Metrics Inc.) and Byologic<sup>TM</sup> software (Version 4.0; Protein Metrics Inc.). The glycopeptide fragmentation data were evaluated manually for each glycopeptide; the peptide was scored as true-positive when the correct b and y fragment ions were observed along with oxonium ions corresponding to the glycan identified. The MS data was searched using the Protein Metrics 305 N-glycan library with sulfated glycans added manually. The relative amounts of each glycan at each site as well as the unoccupied proportion were determined by comparing the extracted chromatographic areas for different glycotypes with an identical peptide sequence. The precursor mass tolerance was set at 4 ppm and 10 ppm for fragments. A 1% false discovery rate (FDR) was applied. The relative amounts of each glycan at each site as well as the unoccupied proportion were determined by comparing the extracted ion chromatographic areas for different glycopeptides with an identical peptide sequence.

Glycans were categorized according to the composition detected. HexNAc(2)Hex(10+) was defined as M9Glc, HexNAc(2)Hex(9–5) was classified as M9 to M3. Any of these structures containing a fucose were categorized as FM (fucosylated mannose). HexNAc(3)Hex(5–6)X was classified as Hybrid with HexNAc(3)Fuc(1)X classified as Fhybrid. Complex-type glycans were classified according to the number of processed antenna and fucosylation, HexNAc(3)Hex(3–4)X, HexNAc(4)X, HexNAc(5)X, and HexNAc(6)X is assigned. As this fragmentation method does not provide linkage information compositional isomers are grouped, so for example a triantennary glycan contains HexNAc 5 but so does a biantennary glycans with a bisect. Core glycans refer to truncated structures smaller than M3. M9–M4 were classified as oligomannose-type glycans. Glycans containing at least one sialic acid or one sulfate group were categorized as NeuAc and sulfated respectively. Further, with in complex-type and hybrid-type glycans, glycan compositions have been categorized as, agalactosylated, galactosylated and sialylated. HexNAc(3)Hex(3)X, HexNAc(3)Hex(5)X, HexNAc(4)

XHex( $\leq 3$ ), HexNAc(5)XHex( $\leq 3$ ), and HexNAc(6)XHex( $\leq 3$ ) is assigned as Agalactosylated. HexNAc(3)Hex(4)X and HexNAc(3)Hex(6)X, HexNAc(4)XHex ( $>3$ ), HexNAc(5)XHex ( $> 3$ ), and HexNAc(6)XHex ( $>3$ ) is assigned as galactosylated. The complex-type and hybrid type glycans with NeuAc are assigned as sialylated.

#### QUANTIFICATION AND STATISTICAL ANALYSIS

Statistical analyses were performed in Graphpad Prism v8.0 or later. For comparison between individual groups, unpaired two-tailed Student t-tests were performed. For comparisons between groups over time, two-way ANOVAs were performed. For comparisons of Kaplan-Meier survival curves, Mantel-Cox tests were performed. Details of these statistical tests, as well as information on biological and technical replicates, can be found in the figure captions.